OH-initiated atmospheric degradation of hydroxyalkyl hydroperoxides: mechanism, kinetics, and structure-activity relationship

Long Chen,[1,2] Yu Huang, *[,1,2] Yonggang Xue, [1,2] Zhihui Jia,[3] Wenliang Wang[4]

[1] *State Key Lab of Loess and Quaternary Geology (SKLLQG), Institute of Earth Environment, Chinese Academy of Sciences (CAS), Xi'an, 710061, China*

[2] *CAS Center for Excellence in Quaternary Science and Global Change, Xi'an, 710061, China*

[3] *School of Materials Science and Engineering, Shaanxi Normal University, Xi'an, Shaanxi, 710119, China*

[4] *School of Chemistry and Chemical Engineering, Key Laboratory for Macromolecular Science of Shaanxi Province, Shaanxi Normal University, Xi'an, Shaanxi, 710119, China*

Submitted to *Atmospheric Chemistry & Physics*

*Corresponding author:

Prof. Yu Huang, E-mail address: huangyu@ieecas.cn

Abstract:

Hydroxyalkyl hydroperoxides (HHPs), formed in the reactions of Criegee intermediates (CIs) with water vapour, play essential roles in the formation of secondary organic aerosol (SOA) under atmospheric conditions. However, the transformation mechanism for OH-initiated oxidation of HHPs is remain incompletely understood. Herein, the quantum chemical and kinetics modeling methods are applied to insight into the detailed mechanisms of OH-initiated oxidation of distinct HHPs ($HOCH_2OOH$, $HOCH(CH_3)OOH$ and $HOC(CH_3)_2OOH$) formed from the reactions of CH_2OO, *anti*-CH_3CHOO and $(CH_3)_2COO$) with water vapor. The calculations show that the dominant pathway is the H-abstraction from the -OOH group in the initiation reactions of OH radical with $HOCH_2OOH$ and $HOC(CH_3)_2OOH$. H-abstraction from -CH group is competitive with that from the -OOH group in the reaction of OH radical with $HOCH(CH_3)OOH$. The barrier of H-abstraction from the -OOH group is slightly increased as the number of methyl group is increased. In pristine environments, the self-reaction of RO_2 radical initially produces tetroxide intermediate via an oxygen-to-oxygen coupling, then it decomposes into propagation and termination products through the asymmetric two-step O-O bond scission, in which the rate-limiting step is the first O-O bond cleavage. The barrier height of distinct RO_2 radicals reactions with HO_2 radical is independent on the number of methyl substitution. In urban environments, reaction with O_2 forming formic acid and HO_2 radical is the dominant removal pathway for $HOCH_2O$ radical formed from the reaction of $HOCH_2OO$ radical with NO. The β-site C-C bond scission is the dominate pathway in the dissociation of $HOCH(CH_3)O$ and $HOC(CH_3)_2O$ radicals formed from the $HOCH(CH_3)OO\cdot$ + NO and $HOC(CH_3)_2OO\cdot$ + NO reactions. These new findings are expected to deepen our current understanding for the photochemical oxidation of hydroperoxides under realistic atmospheric conditions.

1. Introduction

Hydroxyalkyl hydroperoxides (HHPs), formed in the reactions of Criegee intermediates (CIs) with water vapour and in the initiation OH-addition with subsequent HO_2-termination reactions, play important roles in the formation of secondary organic aerosol (SOA) (Qiu et al., 2019; Kumar et al., 2014). The CIs formed from the ozonolysis of alkenes are characterized by high reactivity and excess energies, which can proceed either prompt unimolecular decay to OH radical or, after collisional stabilization, bimolecular reactions with various trance gases like SO_2, NO_2 and H_2O to produce sulfate, nitrate and SOA, thereby influencing air quality and human health (Lester and Klippenstein, 2018; Chen et al., 2017, 2019; Liu et al., 2019; Chhantyal-Pun et al., 2017; Anglada and Solé, 2016; Gong and Chen, 2021). Among these reactions, the bimolecular reaction of CIs with water is thought to be the dominant chemical sink because its concentration (1.3-8.3 $\times 10^{17}$ molecules cm^{-3}) is several orders of magnitude greater than those of SO_2 and NO_2 (~ 10^{12} molecules cm^{-3}) in the atmosphere (Huang et al., 2015; Khan et al., 2018; Taatjes et al., 2013, 2017). The primary products of CIs reactivity toward water are highly oxygenated HHPs that are difficult to detect and identify by using the available analytical techniques due to their thermally instability (Qiu et al., 2019; Anglada and Solé, 2016; Chao et al., 2015; Chen et al., 2016a; Ryzhkov and Ariya, 2003).

HHPs, due to the presence of both hydroxyl and perhydroxy moieties, have relatively low volatility contributing substantially to the formation of SOA (Qiu et al., 2019). The atmospheric degradation of HHPs initiated by OH radical is expected to be one of the dominant loss processes because OH radical is the most powerful oxidizing agent (Gligorovski et al., 2015; Allen et al., 2018). Reaction with OH radical includes three possible H-abstraction channels: (a) the alkyl hydrogen, (b) the -OH hydrogen, and (c) the -OOH hydrogen, which is followed by further reactions to generate organic peroxy radicals (RO_2) as reactive intermediates (Allen et al., 2018). Based on our current mechanistic understanding, RO_2 radicals have three possible channels in pristine environments: (1) they can proceed self- and cross-reactions resulting in

formation of alkoxy radical RO, alcohol, carbonyl, accretion products (Berndt et al., 2018; Zhang et al., 2012; Valiev et al., 2019); (2) they can react with HO_2 radical leading to the formation of closed-shell hydroperoxide (ROOH), RO ; OH radical, etc.; (Dillon and Crowley, 2008; Iyer et al., 2018) (3) they can undergo autoxidation via intramolecular H-shift and alternating O_2-addition steps producing highly oxygenated organic molecules (HOMs), which have been identified as the low volatility compounds that contribute to the formation of SOA (Crounse et al., 2013; Jokinen et al., 2014; Wang et al., 2018; Ehn et al., 2014; Iyer et al., 2021). In urban environments, RO_2 radicals can react with NO_x generating peroxynitrate (RO_2NO_2), organic nitrate ($RONO_2$), RO ·and other SOA precursors (Wang et al., 2017; Xu et al., 2014, 2020; Ma et al., 2021). The relative importance of distinct pathways depends strongly on the nature of RO_2 radicals and the concentrations of coreactants.

Hydroxymethyl hydroperoxide (HMHP, $HOCH_2OOH$), the simplest HHPs from the ozonolysis of ethene in the presence of water, is observed in significant abundance in the atmosphere (Allen et al., 2018). The measured concentration of HMHP is varied considerably depending on the location, season and altitude, and its concentration is measured to be up to 5 ppbv in forested regions (Allen et al., 2018; Francisco and Eisfeld, 2009). Recently, the concentration of HMHP was measured during the summer 2013 in the southeastern United States, and found that the average mixing ratio of HMHP is 0.25 ppbv with a maximum of 4.0 ppbv in the boundary layer(Allen et al., 2018). A recent experimental study by Allen et al. (2018) conducted the OH-initiated oxidation of HMHP in an environmental chamber and simulated the impact of HMHP oxidation on the global formic acid concentrations using the chemical transport model GEOS-Chem. It was found that H-abstraction from the methyl group of HMHP results in formic acid, and it contributes to the global formic acid production about 1.7 Tg yr^{-1}. Francisco and Eisfeld (2009) by employing *ab initio* CCSD(T)//MP2 methods, studied the atmospheric oxidation mechanism of HMHP initiated by OH radical, arriving at the same conclusion that the degradation of HMHP could be a new source of formic acid in the atmosphere. Additionally, the unimolecular decomposition of HMHP is another important removal process in the

atmosphere. Chen et al. (2016b) found that the formation of CH_2O and H_2O_2 is more preferable than that of the production of HCOOH and H_2O. Kumar et al. (2014) obtained the same conclusion that the aldehyde- or ketone-forming pathway is kinetically favored over that the carboxylic acid-forming channel in the unimolecular decomposition of a variety of HHPs. All the above milestone investigations offer very useful information for understanding the decomposition of HHPs in the gas phase. However, to the best of our knowledge, there is a few studies on the subsequent transformations of the resulting H-abstraction products formed from the OH-initiated oxidation of larger HHPs. And the effect of the size and number of substituents on the rates and outcomes of SOA precursors (e.g. ROOR, HOMs) is uncertain up to now. Therefore, it is necessary to assess the potential of larger HHPs and their oxidation products to substantial SOA formation under different NO_x conditions.

In this article, we mainly investigate the detailed mechanisms and kinetic properties of distinct HHPs oxidation initiated by OH radical by employing quantum chemical and kinetics modeling methods. For the resulting H-abstraction products RO_2 radicals, the subsequent reactions involving self-reaction, isomerization and reaction with HO_2 radical are taken into account in the absence of NO, while the subsequent reactions including addition, decomposition and H-abstraction by O_2 are considered in the presence of NO. The investigated HHPs in this work are generated from the bimolecular reactions of distinct carbonyl oxides (CH_2OO, *anti*-CH_3CHOO and $(CH_3)_2COO$) with water vapor.

2. Computational details

2.1 Electronic structure and energy calculations

The equilibrium geometries of all the open-shell species, including reactants (R), pre-reactive complex (RC), transition state (TS), post-reactive complex (PC), and products (P), are fully optimized at the unrestricted M06-2X/6-311+G(2df,2p) level of theory (UM06-2X) (Zhao and Truhlar, 2006; Zheng and Truhlar, 2009), whereas all the closed-shell species are optimized at the restricted M06-2X/6-311+G(2df,2p) level of theory (RM06-2X). This is because the M06-2X functional has been proven to

produce reliable performance for describing thermochemistry, kinetics and non-covalent interactions (Zhao and Truhlar, 2008). Harmonic vibrational frequencies are performed at the same level to verify that each stationary point is either a true minima (with no imaginary frequency) or a transition state (with one imaginary frequency). Zero-point vibrational energy (ZPVE) and Gibbs free energies corrections (G_{corr}) from harmonic vibrational frequencies are scaled by a factor of 0.98 (Zhao and Truhlar, 2006). The intrinsic reaction coordinate (IRC) calculations are performed to verify the connection between the transition state and the designated reactant and product (Fukui, 1981). The single-point energies are calculated at the (U/R)M06-2X/ma-TZVP level of theory (Zheng, et al., 2011).

The tetroxide intermediate formed from the self-reaction of RO_2 radical proceeds through the asymmetric two step O-O bond scission to produce a caged tetroxide intermediate of overall singlet multiplicity comprising two same-spin alkoxyl radicals (spin down) and triplet oxygen (spin up). This type of reaction mechanism can be described by the broken symmetry unrestricted DFT (UDFT) and multi-reference CASSCF methods (Lee et al., 2016; Bach et al., 2005). Previous studies have demonstrated that the UDFT method is suitable to identify the metastable singlet caged radical complex minimum and is successfully located the transition states of O-O bond homolysis, and the energies are comparable to the more accurate and expensive CASSCF method (Lee et al., 2016; Bach et al., 2005). In the present study, the UDFT method is selected to study the asymmetric O-O bond scission and represents a compromise between the computational accuracy and efficiency. The broken symmetry UM06-2X/6-311+G(2df,2p) method is applied to generate the initial guesses of the tetroxide intermediate and transition state geometries with mixed HOMO and LUMO ($S^2 \approx 1$) by using the guess = mix keyword. The single-point energies are refined at the UM06-2X/ma-TZVP level of theory.

In order to further evaluate the reliability of the employed method in predicting reaction mechanism, the single-point energies for all the stationary points involved in the initiation reactions of OH radical with distinct HHPs are recalculated at the (U/R)CCSD(T)/6-311+G(2df,2p) level of theory based on the (U/R)M06-2X

optimized geometries. Furthermore, the basis set superposition error (BSSE) is also performed to evaluate the stability of the pre-reactive complexes by employing the counterpoise method (Boys and Bernardi, 1970). For simplicity, no prefix is adopted throughout this article. Herein, the Gibbs free energy (G) for each species is obtained by combining the single-point energy with the Gibbs correction ($G = G_{corr} + E$). The electronic energy ($\Delta E_a^{\#}$) and free energy ($\Delta G_a^{\#}$) barriers are defined as the difference in energy between transition state and pre-reactive complex ($\Delta E_a^{\#} = E_{TS} - E_{RC}$ and $\Delta G_a^{\#} = G_{TS} - G_{RC}$). The reaction free energy (ΔG) is referred to the difference in energy between product and reactant ($\Delta G = G_P - G_R$). The calculated $\Delta E_a^{\#}$ and $\Delta G_a^{\#}$ for the initiation H-abstraction pathways are summarized in Table S1. As shown in Table S1, the mean absolute deviations (MADs) of $\Delta E_a^{\#}$ and $\Delta G_a^{\#}$ between CCSD(T)/6-311+G(2df,2p) and M06-2X/ma-TZVP approaches are 0.43 and 0.45 kcal·mol^{-1}, respectively; the largest deviations of $\Delta E_a^{\#}$ and $\Delta G_a^{\#}$ are 1.2 and 1.1 kcal·mol^{-1}, respectively. These results reveal that the energies obtained from the M06-2X/ma-TZVP method are in very good accord with those from the gold-standard coupled-cluster approach CCSD(T) within the uncertainties of systematic errors. Therefore, the M06-2X/ma-TZVP method is selected to investigate the atmospheric degradation of HHP initiated by OH radical under different conditions. In the following sections, unless otherwise stated, the $\Delta G_a^{\#}$ is applied to construct the reaction profiles.

For the H-shift reactions of peroxy radicals RO_2, reactants, transition states and products have multiple conformers. Previous literatures have demonstrated that the reaction kinetics of multiconformers involvement are more precisely than that of the single conformer approximation (Møller et al., 2016, 2020). Herein, the multiconformers treatment is performed to investigate the H-shift reactions RO_2 radicals. A conformer search within the Molclus program is employed to generate a pool of conformers for RO_2 radicals (Lu, 2020). The selected conformers are further optimized at the M06-2X/6-311+G(2df,2p) level of theory, followed by single-point energies calculations at the M06-2X/ma-TZVP level of theory. On the basis of the calculated Gibbs free energies, the Boltzmann populations (w_i) of each

205 $RO_2 \cdot$conformer is expressed as eqn 1.

206
$$w_i = \frac{e^{-\Delta G_i / k_B T}}{\sum_i e^{-\Delta G_i / k_B T}} \quad (1)$$

207 where ΔG_i is the relative Gibbs free energy of conformer i, k_B is the Boltzmann's
208 constant, T is temperature in Kelvin. All the quantum chemical calculations are
209 performed by using the Gaussian 09 program package (Frisch et al., 2009).

210 ## 2.2 Kinetics calculations

211 The rate coefficients of unimolecular reactions are calculated by using the
212 Rice-Ramsperger-Kassel-Marcus theory coupled with energy-grained master equation
213 (RRKM-ME) method (Holbrook et al., 1996), and the rate coefficients of bimolecular
214 reactions are determined by utilizing traditional transition state theory (TST)
215 (Fernández-Ramos et al., 2007). The RRKM-ME calculations are performed by
216 implementing the MESMER 6.0 program suite (Glowacki et al., 2012). N_2 is used as
217 the buffer gas. The single exponential down model is employed to simulate the
218 collision energy transfer ($<\Delta E>_{down}$ = 200 cm^{-1}). The collisional Lennard-Jones
219 parameters are estimated by using an empirical formula described by Gilbert and
220 Smith (1990). For the H-shift reactions of RO_2 radicals, the rate coefficients are
221 determined by employing the multiconformer transition state theory (MC-TST)
222 approach (Møller et al., 2016). The MC-TST rate coefficient $k_{MC\text{-}TST}$ is calculated by
223 the sum of the individual intrinsic reaction coordinate TST (IRC-TST) rate coefficient
224 $k_{IRC\text{-}TST}$, each weighted by Boltzmann population of corresponding $RO_2 \cdot$ conformer
225 (Møller et al., 2016).

226
$$k_{MC\text{-}TST} = \sum_{i}^{\text{all TS conf.}} w_i \times k_{IRC\text{-}TST i} \quad (2)$$

227 where $k_{IRC\text{-}TST i}$ represents the rate coefficient of conformer i, and w_i is the relative
228 Boltzmann population of the corresponding reactant connected to TS_i. The
229 one-dimensional asymmetry Eckart model is employed to calculate the tunneling
230 correction (Eckart, 1930). Considering the uncertainty in barrier heights (~ 1.0
231 kcal·mol^{-1} by the M06-2X method) and in tunneling corrections, the uncertainty of the

232 calculated rate coefficient is about one order of magnitude in the present study.

233 # 3. Results and discussion

234 ## 3.1 Initiation reaction of HHPs with OH radical

235 Previous literatures have proposed that the lifetime of CI with respect to the
236 reaction with water vapour exhibits a highly dependent on the nature of CIs (Anglada
237 and Solé, 2016; Taatjes et al., 2013; Anglada et al., 2011), and the primary product is
238 HHPs in both gas phase and air/water interface (Chao et al., 2015; Chen et al., 2016a;
239 Smith et al., 2015; Zhu et al., 2016; Zhong et al., 2018). In the present study, we
240 mainly consider three kinds of HHPs originated from the addition of water to CH_2OO
241 and methyl-substituted CI (*anti*-CH_3CHOO and $(CH_3)_2COO$). The lowest-energy
242 conformers HHP ($HOCH_2OOH$, $HOCH(CH_3)OOH$ and $HOC(CH_3)_2OOH$) are
243 obtained from the previous study as shown in Figure 1 (Chen et al., 2019), and they
244 are selected as model system to investigate the atmospheric degradation mechanism
245 of HHP initiated by OH radical. Letters and numbers are applied to mark carbon,
246 oxygen and hydrogen atoms in different reaction sites.

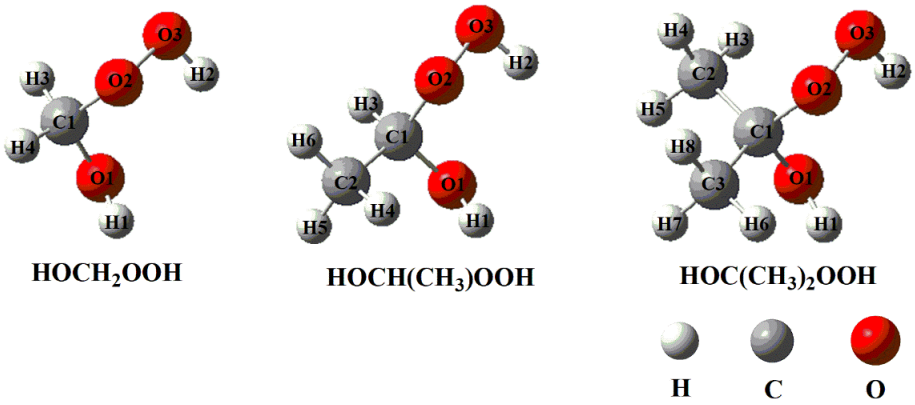

247
248 **Figure 1.** The structures of distinct HHPs

249 The free-energy and electronic-energy potential energy surfaces (PESs) for the
250 initiation reactions of OH radical with $HOCH_2OOH$, $HOCH(CH_3)OOH$ and
251 $HOC(CH_3)_2OOH$ are presented in Figures 2-4 and S1-S3, respectively. And the
252 optimized geometries of all the stationary points are displayed in Figures S6-S8,
253 respectively. As can be seen in Figure 2, the reaction for $HOCH_2OOH$ with OH
254 radical proceeds via four distinct pathways: H-abstraction from the $-O_1H_1$ (R1), $-C_1H_3$

(R2), -C_1H_4 (R3) and -$O_2O_3H_2$ groups (R4). For each pathway, a pre-reactive complex with a six- or seven-membered ring structure is formed in the entrance channel, which is stabilized by hydrogen bond interactions between the oxygen atom of OH radical and the abstraction hydrogen atom of $HOCH_2OOH$, and the remnant hydrogen atom of OH radical and one of oxygen atoms of $HOCH_2OOH$ (Figure S6). Then, it surmounts modest barrier that is higher in energy than the reactants to reaction. The reaction barrier $\Delta G_a^{\#}$ are reduced in the order of 6.4 (R1) > 5.8 (R2) ≈ 5.4 (R3) > 1.5 (R4) kcal mol^{-1}, indicating that H-abstraction from the -$O_2O_3H_2$ group (R4) is more preferable than those from the -O_1H_1, -C_1H_3 and -C_1H_4 groups (R1-R3). Same conclusion is also derived from the energy barriers $\Delta E_a^{\#}$ that R4 is the most favorable H-abstraction pathway (Figure S1). The difference of barrier heights can be attributed to the bond dissociation energy (BDE) of different types of bonds in $HOCH_2OOH$ molecule. The BDE are decreased in the order of 103.7 (O_1-H_1) > 98.2 (C_1-H_3) ≈ 97.4 (C_1-H_4) > 87.2 (O_3-H_2) kcal mol^{-1}, which are in good agreement with the order of barrier heights of H-abstraction reactions. As indicated by their reaction free energy values, it can be found that the exothermicity of R4 is the largest among these four H-abstraction reactions. Based on the above discussions, it is concluded that H-abstraction from the -$O_2O_3H_2$ group resulting in formation of $HOCH_2OO$ radical (R4) is feasible on both thermodynamically and kinetically.

Considering the different reaction sites of hydrogen atoms, the atmospheric transformation of $HOCH(CH_3)OOH$ from the *anti*-CH_3CHOO + H_2O reaction should have six types of H-abstraction pathways as presented in Figure 3. As shown in Figure 3, each H-abstraction reaction begins with the formation of a weakly bound hydrogen bonded pre-reactive complex with a six- or seven-membered ring structure in the entrance channel (Figure S7). Then it immediately transforms into the respective product via the corresponding transition state. The $\Delta G_a^{\#}$ of H-abstraction from the -C_1H_3 (R6) and -$O_2O_3H_2$ (R8) groups are 2.2 and 1.7 kcal mol^{-1}, respectively, which are ~ 4-5 kcal mol^{-1} lower than those from the -O_1H_1 (R5) and -CH_3 groups (R7). This result shows that R6 and R8 have nearly identical importance in the atmosphere. Compared with the barriers of H-abstraction at the C_α (R6) and C_β (R7) positions, it

can be found that the former case is more favourable than the latter case. This conclusion is further supported by Jara-Toro's study for the reactions of OH radical with linear saturated alcohols (methanol, ethanol and n-propanol) that H-abstraction at the C_α position is predominant (Jara-Toro, R. A et al., 2017, 2018).

For the OH-initiated oxidation of $HOCH(CH_3)OOH$ from the *syn*-CH_3CHOO + H_2O reaction, the corresponding free-energy and electronic-energy PESs are displayed in Figures S4 and S5, respectively. From Figure S4, it can be seen the H-abstraction by OH radical from $HOCH(CH_3)OOH$ has six kinds of pathways. For each pathway, a per-reactive complex is formed prior to the corresponding transition state, and then it overcomes modest barrier to reaction. The $\Delta G_a^{\#}$ of R6' and R8' are 2.3 and 1.8 kcal·mol^{-1}, respectively, which are about 5 kcal·mol^{-1} lower than those of R5' and R7'. This result shows that H-abstraction from the -CH (R6') and -OOH (R8') groups are preferable kinetically. Same conclusion is also derived from the energy barriers $\Delta E_a^{\#}$ that the R6' and R8' the most favourable H-abstraction pathways (Figure S5). It should be noted that although the barriers of R6' and R8' are comparable, the exoergicity of the former case is significantly lower than that of the latter case. The above-mentioned conclusions are consistent with the results derived from the OH-initiated oxidation of $HOCH(CH_3)OOH$ from the *anti*-CH_3CHOO + H_2O reaction. Zhou et al. has demonstrated that the bimolecular reaction of *syn*-CH_3CHOO with water leading to the formation of $HOCH(CH_3)OOH$ is of less importance in the atmosphere, while the unimolecular decay to OH radical is the major loss process of *syn*-CH_3CHOO (Zhou et al., 2019). Therefore, in the present study, we mainly focus on the subsequent mechanism of intermediate generated from OH-initiated oxidation of $HOCH(CH_3)OOH$ from the *anti*-CH_3CHOO + H_2O reaction.

From Figure 4, it can be seen that H-abstraction from $HOC(CH_3)_2OOH$ includes eight possible H-abstraction pathways. All the H-abstraction reactions are strongly exothermic and spontaneous, signifying that they are thermodynamically feasible under atmospheric conditions. It deserves mentioning that the release of energy of R12 is significantly greater than those of R9-R11. For each H-abstraction pathway, a RC with a six- or seven-membered ring structure is formed prior to the

corresponding TS, which is more stable than the separate reactants due to the hydrogen bond interactions between $HOC(CH_3)_2OOH$ and OH radical. Then, the RC overcomes modest barrier to reaction. The $\Delta G_a^{\#}$ of H-abstraction from the $-O_2O_3H_2$ group (R12) is 2.7 kcal mol^{-1}, which is the lowest among these eight H-abstraction reactions. This result again shows that the H-abstraction from the $-O_2O_3H_2$ group is the dominant pathway.

The rate coefficients of every H-abstraction pathway involved in the initiation reactions of distinct HHPs with OH radical are estimated over the temperature range from 273 to 400 K as summarized in Table S2-S4 and Figures S9-S11. As shown in Table S2, the total rate coefficients k_{tot} of $HOCH_2OOH$ reaction with OH radical are slightly decreased with the temperature increasing. At ambient temperature, k_{tot} is estimated to be 3.3×10^{-11} cm^3 $molecule^{-1}$ s^{-1}, which is a factor of ~5 greater than the Allen's result ($(7.1 \pm 1.5) \times 10^{-12}$ cm^3 $molecule^{-1}$ s^{-1}, at 295 K) derived from the reaction of HMHP with OH radical by using the CF_3O^- chemical ionization mass spectrometry (CIMS) and laser-induced fluorescence (LIF) (Allen et al., 2018). Such a discrepancy could be attributed to the uncertainty in barrier height and tunneling correction. $k_{R4(O3\text{-}H2)}$ is 1-2 orders of magnitude greater than $k_{R1(O1\text{-}H1)}$, $k_{R2(C1\text{-}H3)}$ and $k_{R3(C1\text{-}H4)}$ in the whole temperature range, implying that R4 is the most favorable H-abstraction pathway. For example, $k_{R4(O3\text{-}H2)}$ is calculated to be 2.9×10^{-11} cm^3 $molecule^{-1}$ s^{-1} at 298 K, which is higher than $k_{R1(O1\text{-}H1)}$ (1.8×10^{-13}), $k_{R2(C1\text{-}H3)}$ (9.9×10^{-13}) and $k_{R3(C1\text{-}H4)}$ (2.0×10^{-12}) by 161, 29 and 15 times, respectively.

From Table S3, it can be seen that the total rate coefficients k'_{tot} of $HOCH(CH_3)OOH$ reaction with OH radical are decreased in the range of 4.5×10^{-11} (273 K) to 8.1×10^{-12} (400 K) cm^3 $molecule^{-1}$ s^{-1} with increasing temperature, and they exhibit a slightly negative temperature dependence. $k_{R8(O3\text{-}H2)}$ are approximately identical to k'_{tot} in the entire temperature range, which are 1-2 orders of magnitude greater than $k_{R5(O1\text{-}H1)}$, $k_{R6(C1\text{-}H3)}$, $k_{R7\text{-}1(C2\text{-}H4)}$, $k_{R7\text{-}2(C2\text{-}H5)}$ and $k_{R7\text{-}3(C2\text{-}H6)}$. The result again shows that H-abstraction from the -OOH group (R8) is preferable kinetically. It should be noted that although the barriers of R8 and R6 are comparable, $k_{R8(O3\text{-}H2)}$ is about one order of magnitude higher than $k_{R6(C1\text{-}H3)}$ over the temperature range studied.

The reason is most likely due to the stability of pre-reactive complexes that IM8-a is more stable than IM6-a in energy. A similar conclusion is derived from the results of rate coefficient of $HOC(CH_3)_2OOH$ + OH reaction that H-abstraction from the -OOH group (R12) is favorable kinetically (Table S4). The concentrations of OH radical vary from 5 to 15 $\times 10^6$ molecules cm^{-3} during daylight (Long et al., 2017), resulting in the atmospheric lifetime of $HOCH_2OOH$, $HOCH(CH_3)OOH$ and $HOC(CH_3)_2OOH$ reactivity toward OH radical are estimated to be 0.58-1.74 h, 0.60-1.79 h and 1.23-3.69 h at room temperature.

In summary, the dominant pathway is the H-abstraction from the -OOH group in the initiation reactions of OH radical with $HOCH_2OOH$. H-abstraction from -CH group is competitive with that from the -OOH group in the reaction of OH radical with $HOCH(CH_3)OOH$. Compared the barriers of H-abstraction from the -OOH and $-CH_2$ groups in the OH + $HOCH_2OOH$ system with that for the analogous reactions in the OH + $HOCH(CH_3)OOH$ system. It can be found that the barrier of H-abstraction from the -CH group is reduced by 3.6 kcal mol^{-1}, whereas the barrier of H-abstraction from the -OOH group is increased by 0.2 kcal mol^{-1} when a methyl group substitution occurs at the C1-position of $HOCH_2OOH$. The dominant pathway is the H-abstraction from the -OOH group in the reaction of OH radical with $HOC(CH_3)_2OOH$, and the barrier height is increased by 1.2 kcal mol^{-1} compared to the OH + $HOCH_2OOH$ system. The barrier of H-abstraction from the -OOH group is slightly increased as the number of methyl group is increased. It is interesting to compare the rate coefficient of dominant pathway in the OH + $HOCH_2OOH$ system with that for the analogous reactions in the OH + $HOCH(CH_3)OOH$ and OH + $HOC(CH_3)_2OOH$ reactions. It can be found that the rate coefficient is almost identical when a methyl group substitution occurs at the C_1-position, whereas the rate coefficient reduces by a factor of 2-5 when two methyl groups introduce into the C_1-position.

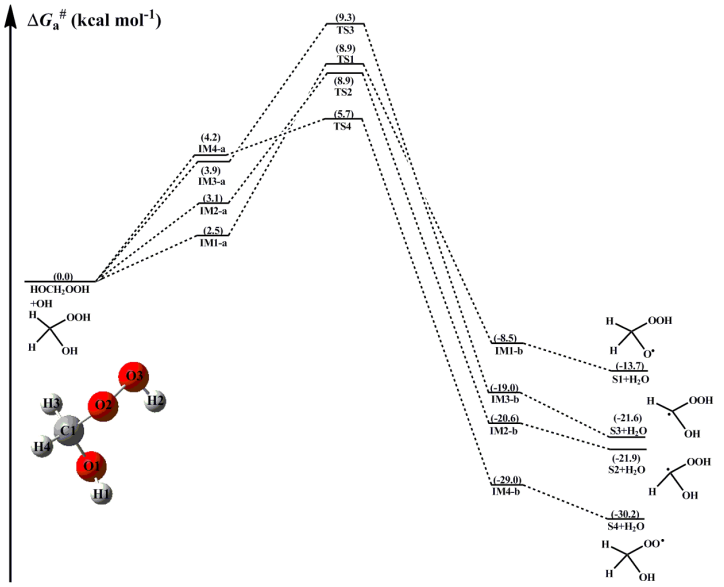

Figure 2. PES ($\Delta G_a^{\#}$) for the OH-initiated reactions of $HOCH_2OOH$ from the CH_2OO + H_2O reaction predicted at the M06-2X/ma-TZVP//M06-2X/6-311+G(2df,2p) level of theory (a and b represent the pre-reactive and post-reactive complexes)

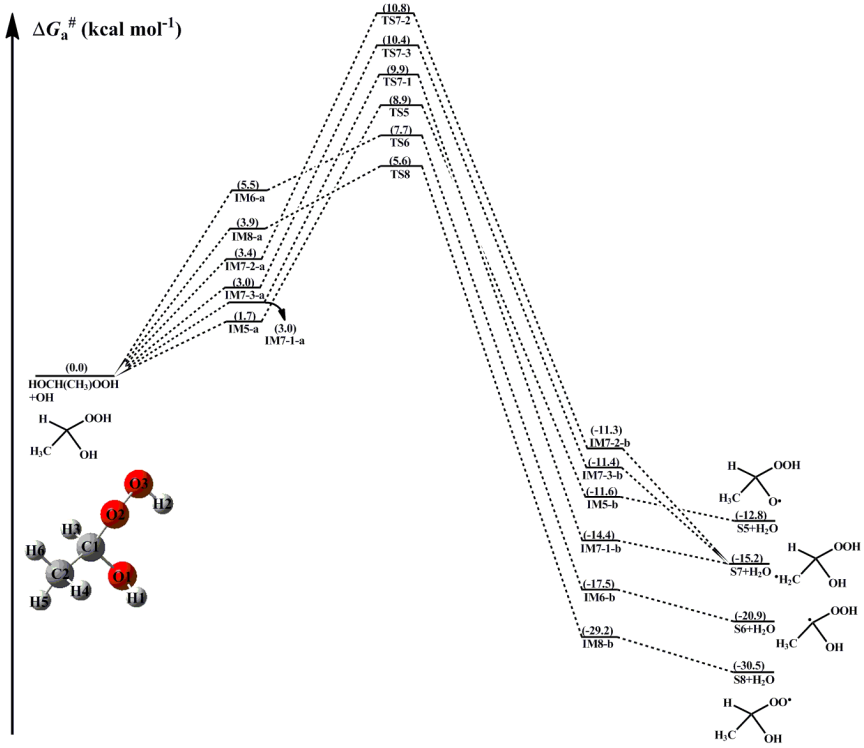

Figure 3. PES ($\Delta G_a^{\#}$) for the OH-initiated reactions of $HOCH(CH_3)OOH$ from the *anti*-CH_3CHOO + H_2O reaction predicted at the M06-2X/ma-TZVP//M06-2X/6-311+G(2df,2p) level of theory (a and b represent the pre-reactive and post-reactive complexes)

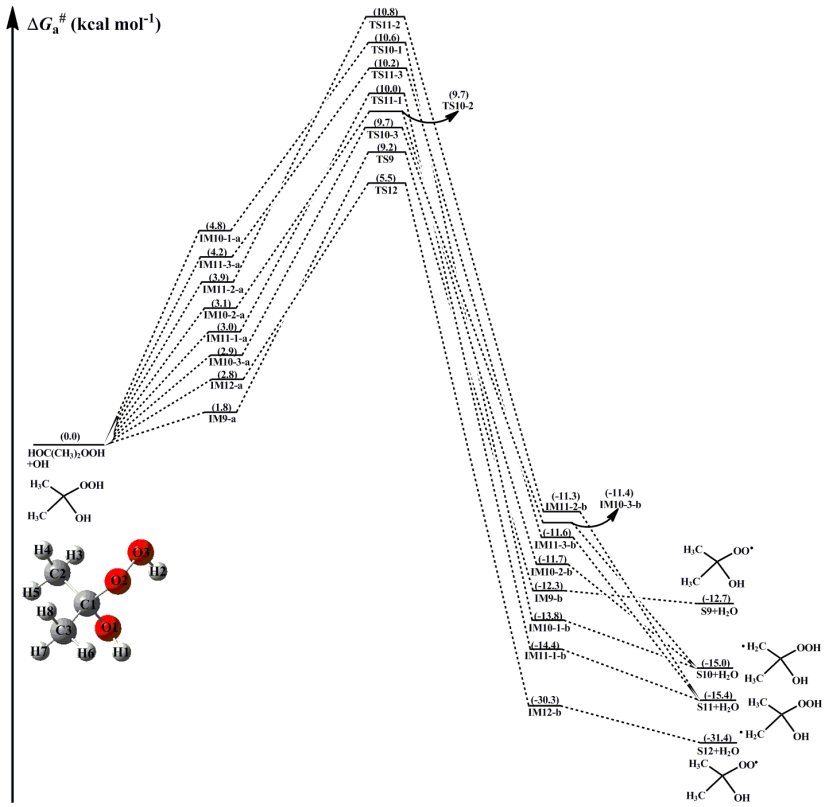

Figure 4. PES ($\Delta G_a^{\#}$) for the OH-initiated reactions of $HOC(CH_3)_2OOH$ from the $(CH_3)_2COO$ + H_2O reaction predicted at the M06-2X/ma-TZVP//M06-2X/6-311+G(2df,2p) level of theory (a and b represent the pre-reactive and post-reactive complexes)

3.2 Subsequent reactions of H-abstraction products RO_2 radicals in pristine environment

In principle, the H-abstraction products RO_2 radicals have three types of channels in pristine environment: (1) the self-reactions of RO_2 radicals can either produce RO ·+ R'O ·+ O_2 (propagation channel), or generate ROH + R'(-H, =O) + O_2 or produce ROOR + O_2 (termination channel) that has been recognized as an important SOA precursor (Berndt et al., 2018; Zhang et al., 2012); (2) RO_2 radicals react with HO_2 radical leading to the formation of hydroperoxide ROOH, alcohol, OH and other products (Winiberg et al., 2016; Chen et al., 2021); (3) RO_2 radicals autoxidation through intramolecular H-shift and alternating O_2 addition steps generate HOMs (Ehn et al., 2014; Bianchi et al., 2019; Nozière and Vereecken, 2019; Rissanen et al., 2014). The relevant details for these three kinds of reactions will be discussed in the following paragraph.

3.2.1 Reactions mechanism for the self-reaction of RO_2 radicals

The self-reaction is one of dominant removal pathways for RO_2 radicals when the concentration of NO is low. The self-reaction of RO_2 radicals usually follows the Russell mechanism (Russell, 1957), and mainly includes four kinds of pathways: (1) $2RO_2 \cdot \rightarrow 2RO \cdot + O_2$; (2) $2RO_2 \cdot \rightarrow ROH + RCO + O_2$; (3) $2RO_2 \cdot \rightarrow ROOR + O_2$; (4) $2RO_2 \cdot \rightarrow ROOH + R'CHOO$ (Atkinson and Arey, 2003). The relative importance of different pathways varies considerably depending on the nature of RO_2 radicals (Valiev et al., 2019; Lee et al., 2016). A schematic PES for the self-reaction of $HOCH_2OO$ radical is drawn in Figure 5. As can be seen in Figure 5a, the self-reaction of $HOCH_2OO$ radical starts with the formations of tetroxide complexes IM13-a and IM14-a in the entrance channel, with 2.9 and 3.4 kcal mol^{-1} stability. Then they fragment into dimer S13 + $^1O_2$ (R13) and $HOCH_2OOH$ + HOCHOO (R14) via transition states TS13 and TS14 with the barriers of 43.3 and 51.5 kcal mol^{-1}. But the barriers of R13 and R14 are extremely high, making them irrelevant in the atmosphere.

From Figure 5b, it is seen that the self-reaction of $HOCH_2OO$ radical proceeds via oxygen-to-oxygen coupling leading to the formation of tetroxide intermediate S14 with the electronic energy and free energy barriers of 7.3 and 19.6 kcal mol^{-1}. Kumar and Francisco reported that the electronic energy barrier of the gas phase decomposition of $HOCH_2OO$ radical is 14.0 kcal mol^{-1} and it could be a new source of HO_2 radical in the troposphere (Kumar and Francisco, 2015, 2016). Compared with the electronic energy barriers of unimolecular dissociation of $HOCH_2OO$ radical and its self-reaction, it can be found that the self-reaction of $HOCH_2OO$ radical resulting in formation of S14 is significantly feasible. The formed S14 can fragment into $HOCH_2O \cdot$ + HCOOH + $HO_2 \cdot$ via a concerted process of O_2-O_3 and O_5-O_6 bonds rupture and O_3-H_6 bond forming with the barrier of 29.8 kcal mol^{-1}. Alternatively, S14 can convert into the caged tetroxide intermediate S16 through the asymmetric two step O_2-O_3 and O_5-O_6 bonds scission with the barriers of 19.1 and 3.1 kcal mol^{-1}, respectively. The result shows that the latter pathway is more preferable than the

former channel owing to its lower barrier. The overall spin multiplicity of S16 is singlet, in which the O_2 moiety maintains the triplet ground state (spin up) and is very loosely bound. In order to preserve the overall singlet multiplicity, the two $HOCH_2O$ radical pairs ($^3(HOCH_2O\cdots HOCH_2O)$) must have the triplet multiplicity (spin down). S16 could be regarded as the ground state $^3O_2$ moving away from the two $HOCH_2O$ radical pairs that keep interacting. Due to the difficulty in performing the constrained optimization for the dissociation of S16, the $^3O_2$ moiety is considered as a leaving moiety away from two $HOCH_2O$ radical pairs, and merely the dissociation of $^3(HOCH_2O\cdots HOCH_2O)$ is taken into consideration in the present study. It has three types of pathways: (1) it yields $HOCH_2OH$ and excited-state ^3HCOOH through the alpha hydrogen transfer with the barrier of 14.0 kcal·mol^{-1} and 10.2 kcal·mol^{-1} exothermicity, followed by the excited ^3HCOOH to go back to the ground-state ^1HCOOH; (2) it generates two $HOCH_2O$ radicals via the barrierless process with the exoergicity of 16.9 kcal·mol^{-1}; (3) it produces dimer S17 via an intersystem crossing (ISC) step with the exoergicity of 32.1 kcal·mol^{-1}. Based on the calculated reaction barriers, it can be found that the rate-limiting step is the cleavage of O_2-O_3 bond (R17) in the unimolecular decay processes of S14. This conclusion coincides with the previous result obtained from the dissociation of di-t-butyl tetroxide that the rate-controlling step is the rupture of single O-O bond (Lee et al., 2016). Valiev et al. proposed that the ISC rate of ROOR dimer formed from the different $(RO\cdots R'O)$ systems is extremely rapid (> 10^8 s^{-1}) and exhibits a strong stereoselectivity (Valiev et al., 2019).

Figure 6 depicts a schematic PES for the self-reaction of $HOCH(CH_3)OO$ radical. As shown in Figure 6a, the self-reaction of $HOCH(CH_3)OO$ radical can either produce dimer S18 along with $^1O_2$ via transition state TS20 with the barrier of 44.4 kcal·mol^{-1}, or generate $HOCH(CH_3)OOH$ and $HOC(CH_3)OO$ though transition state TS21 with the barrier of 54.3 kcal·mol^{-1}. But the barriers of R20 and R21 are significantly high, making them are of less importance in the atmosphere. Alternatively, the self-reaction of $HOCH(CH_3)OO$ radical proceeds via an oxygen-to-oxygen coupling resulting in formation of tetroxide intermediate S19 with

the barrier of 19.9 kcal mol^{-1} (Figure 6b). The formed S19 proceeds through the asymmetric two step O_2-O_3 and O_5-O_6 bonds scission to produce a caged tetroxide intermediate S21 of overall singlet multiplicity comprising two same-spin alkoxyl radicals (spin down) and triplet oxygen (spin up). These two processes accompany with the barriers of 21.4 and 1.3 kcal mol^{-1}, respectively. Then it decomposes into the propagation ($2HOCH(CH_3)O\cdot + {}^3O_2$) and termination products ($HOCH(CH_3)OH + {}^3CH_3OOH + {}^3O_2$ and dimer S22 + ${}^3O_2$) with the exoergicity of 12.5, 11.7 and 33.0 kcal mol^{-1}. The rate-determining step is the rupture of O_2-O_3 bond (R24) in the dissociation processes of S19.

As shown in Figure 7, the dominant pathway for the self-reaction of $HO(CH_3)_2COO$ radical begins with the formation of tetroxide intermediate S24 via an oxygen-to-oxygen coupling transition state TS28 with the barrier of 20.4 kcal mol^{-1}; then it transforms into the caged tetroxide intermediate S26 of overall singlet spin multiplicity through the asymmetric two-step O-O bond cleavage with the barriers of 22.0 and 3.4 kcal mol^{-1}; finally, S26 can either produce two $HO(CH_3)_2CO$ radicals with the exoergicity of 10.3 kcal mol^{-1}, or generate dimer S27 with the exothermicity of 31.5 kcal mol^{-1}. Different the self-reactions of $HOCH_2OO$ and $HOCH(CH_3)OO$ radicals, the termination product of the self-reaction of $HOC(CH_3)_2OO$ radical is exclusively dimer S27. The reason is due to the absence of alpha hydrogen atom in $HOC(CH_3)_2OO$ radical. Compared with the barrier of rate-determining route R17 in the self-reaction of $HOCH_2OO$ radical, it can be found that the barrier of rate-limiting step R29 is increased by about 3.0 kcal mol^{-1} when two methyl substitutions introduce into the C1-position of $HOCH_2OO$ radical. The reason might be attributed to the cage escape of alkoxyl radicals. It is therefore that the tertiary RO_2 radicals have great opportunity to react with HO_2 radical or autoxidation in pristine environment.

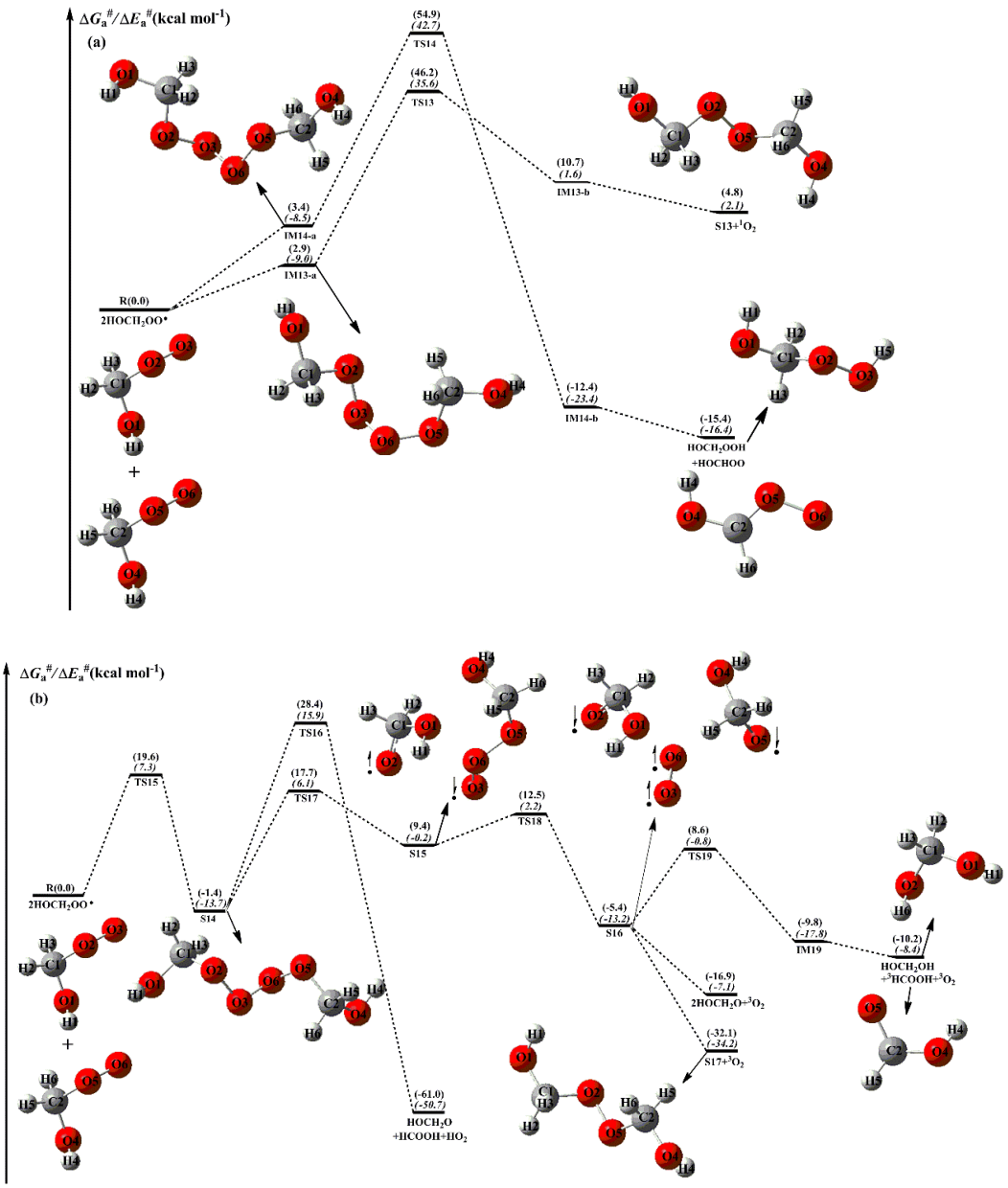

Figure 5. PES ($\Delta G_a^{\#}$ and $\Delta E_a^{\#}$, in italics) for the self-reaction of $HOCH_2OO$ radicals predicted at the M06-2X/ma-TZVP//M06-2X/6-311+G(2df,2p) level of theory

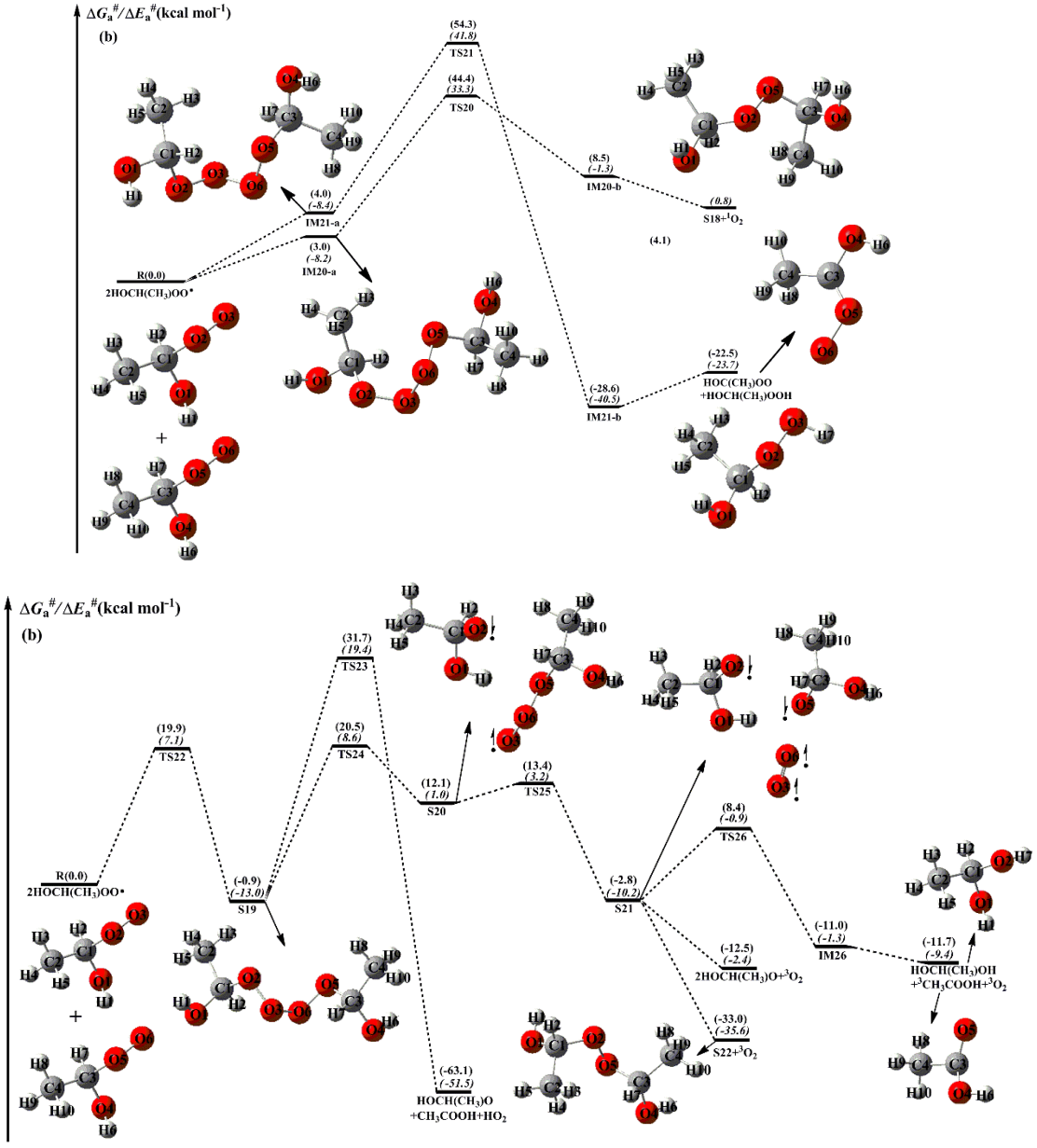

Figure 6. PES ($\Delta G_a^{\#}$ and $\Delta E_a^{\#}$, in italics) for the self-reaction of $HOCH(CH_3)OO$ radicals predicted at the M06-2X/ma-TZVP//M06-2X/6-311+G(2df,2p) level of theory

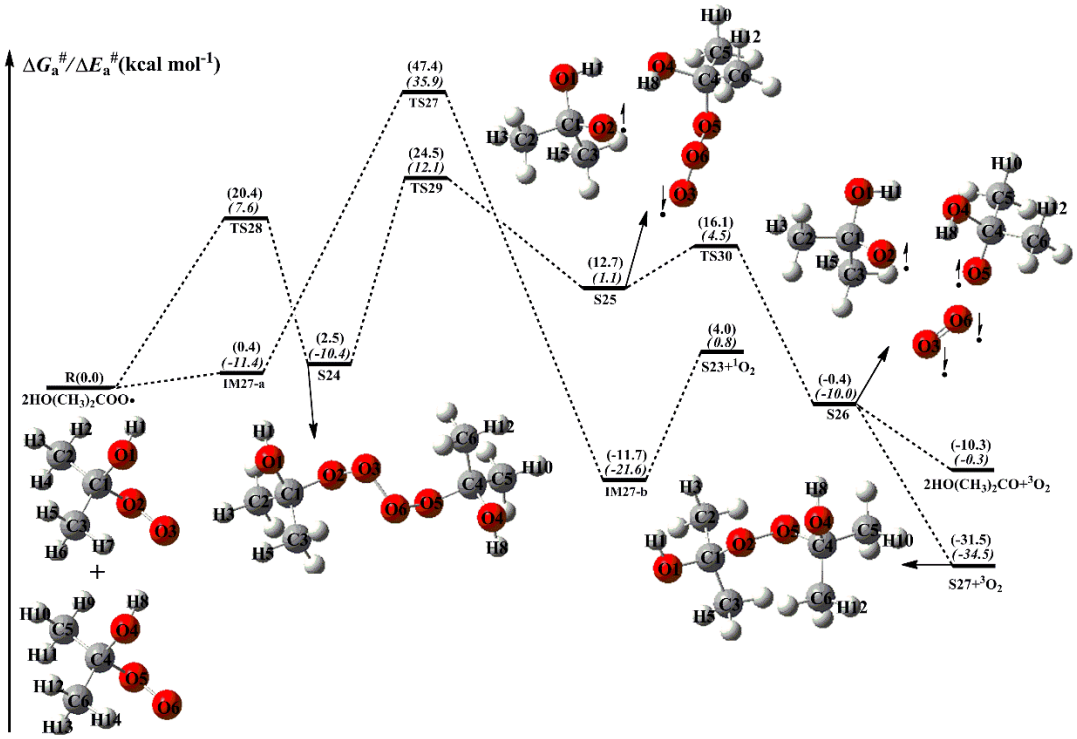

Figure 7. PES ($\Delta G_a^{\#}$ and $\Delta E_a^{\#}$, in italics) for the self-reaction of $HO(CH_3)_2COO$ radicals predicted at the M06-2X/ma-TZVP//M06-2X/6-311+G(2df,2p) level of theory

3.2.2 Reactions mechanism for the reaction of RO_2 radicals with HO_2 radical

When NO is present in low concentration, the bimolecular reaction of RO_2 radicals with HO_2 radical is generally expected to be the dominant pathway as the main product hydroperoxide ROOH. The main sources of HO_2 radical involve the photo-oxidation of oxygenated volatile organic compounds (OVOCs) and the ozonolysis reaction, as well as senondary sources include the reactions of OH radical with CO, ozone and volatile organic compounds (VOCs), the reaction of alkoxy radical RO with O_2 and the red-light-induced decomposition of α-hydroxy methylperoxy radical $OHCH_2OO$ (Kumar et al., 2015; Stone et al., 2012; Hofzumahaus et al., 2009). The atmospheric concentration of HO_2 radical is 1.5-10 × 10^8 molecules cm^{-3} at ground level in polluted urban environments (Stone et al., 2012). A schematic PES for the reactions of distinct RO_2 radicals with HO_2 radical is presented in Figure 8. As shown in Figure 8, all the reactions are strongly exothermic and spontaneous, indicating that they are feasible thermodynamically in the atmosphere. The reaction for $HOCH_2OO\cdot$ with $HO_2\cdot$ (R31) starts with the formation

of a pre-reactive complex IM31-a in the entrance channel, which is more stable than the separate reactants by 3.8 kcal mol^{-1} in energy. Then it converts into $HOCH_2OOH$ and O_2 via a hydrogen atom transfer from the HO_2 radical to the terminal oxygen atom of $HOCH_2OO$ radical with the barrier of 2.0 kcal mol^{-1}. The mechanism of $HOCH(CH_3)OO\cdot + HO_2\cdot$(R32) and $HO(CH_3)_2COO\cdot + HO_2\cdot$(R33) reactions is quite similar to that of $HOCH_2OO\cdot + HO_2\cdot$system. In order to avoid redundancy, we will not discuss them in detail. It deserves mentioning that the barrier height is only reduced by 0.1 kcal mol^{-1} when one or two methyl substitutions occur at the C1-position of $HOCH_2OO$ radical, compared to the barrier of $HOCH_2OO\cdot + HO_2\cdot$reaction. This result implies that the barrier height is not seem to be influenced by the number of methyl substitution. The rate coefficients of distinct RO_2 radicals reactions with HO_2 radical are summarized in Table S5 and Figure S12. As shown in Table S5, the rate coefficients k_{R31} of $HOCH_2OO\cdot + HO_2$ reaction vary from 3.1×10^{-11} (273 K) to 2.1×10^{-12} cm^3 $molecule^{-1}$ s^{-1} (400 K), and they exhibit a negative temperature dependence. Similar conclusion is also obtained from the rate coefficients k_{R32} and k_{R33} that they are decreased with the temperature increasing. It should be noted that the rate coefficient is slightly increased as the number of methyl group is increased. At ambient temperature, k_{R31} is estimated to be 1.7×10^{-11} cm^3 $molecule^{-1}$ s^{-1}, which is in good agreement with the value of $\sim 2 \times 10^{-11}$ cm^3 $molecule^{-1}$ s^{-1} for the reaction of acyl peroxy radicals with HO_2 radical (Wennberg et al., 2018). The typical atmospheric concentrations of HO_2 radical are about 5, 20 and 50 pptv in the urban, rural and forest environments (Bianchi et al., 2019), translating into the pseudo-first-order rate constants $k'_{HO2} = k_{HO2}[HO_2]$ of 1.1×10^{-3}, 4.2×10^{-3} and 1.1×10^{-2} s^{-1}, respectively. The pseudo-first-order rate constants of R32 and R33 are predicted to be 3.0×10^{-3} and 4.8×10^{-3} (urban), 1.1×10^{-2} and 1.8×10^{-2} (rural), 3.0×10^{-2} and 4.8×10^{-2} s^{-1} (forest) at room temperature.

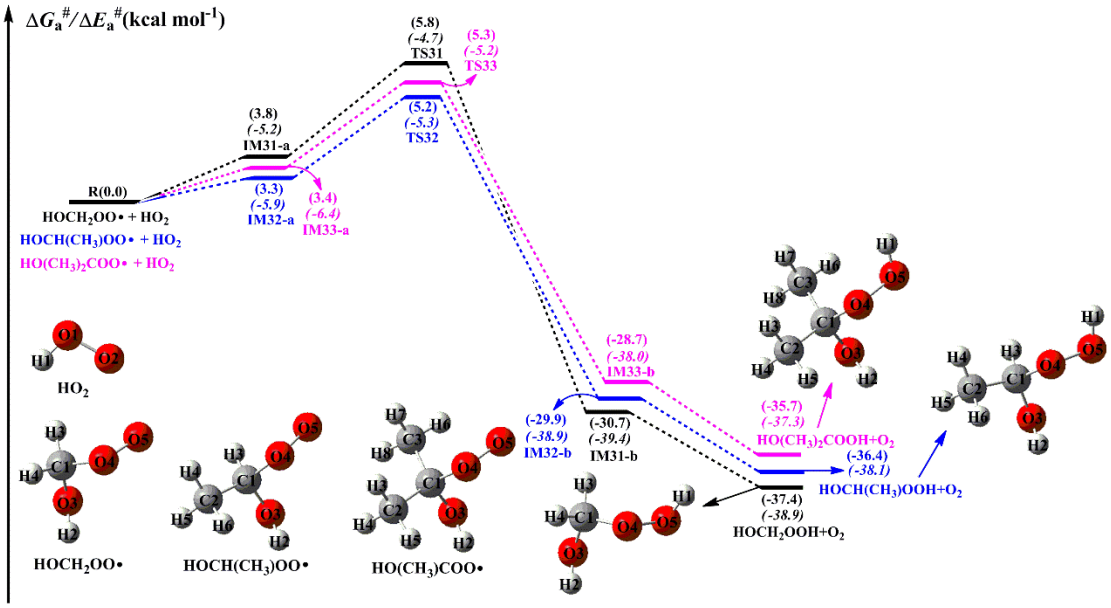

Figure 8. PES ($\Delta G_a^{\#}$ and $\Delta E_a^{\#}$, in italics) for the reactions of HO_2 radical with distinct RO_2 radicals predicted at the M06-2X/ma-TZVP//M06-2X/6-311+G(2df,2p) level of theory

3.2.3 Reactions mechanism for the isomerization of RO_2 radicals

Autoxidation of RO_2 radicals is known to play an important role in the (re)generation of HO_x radicals and in the formation of HOMs (Wang et al., 2017; Bianchi et al., 2019; Rissanen et al., 2014; Ehn et al., 2017). The autoxidation mechanism includes an intramolecular H-shift from the $-CH_3$ or $-CH_2-$ groups to the -OO ·site, resulting in formation of a hydroperoxyalkyl radical QOOH, followed by O_2 addition to form a new peroxy radical ($HOOQO_2$), one after the other, and the resulting finally HOMs (Rissanen et al., 2014; Berndt et al., 2015). For the H-shift reactions of RO_2 radical, reactants, transition states and products have multiple conformers due to the effect of degree of freedom for internal rotation. Based on the calculated results, it can be found that $HOCH_2OO$ radical has four energetically similar conformers ($HOCH_2OO$-a, $HOCH_2OO$-b, $HOCH_2OO$-c and $HOCH_2OO$-d). The relative free energy and Boltzmann population (w_i) of individual conformer are listed in Table S6. As shown in Table S6, the Boltzmann populations of these four conformers are 46.39, 46.31, 2.99 and 4.32%, respectively.

A schematic PES for the H-shift reactions of $HOCH_2OO$ radical is displayed in Figure 9. As can be seen in Figure 9, the lowest-energy conformer $HOCH_2OO$-a can proceed via a 1,3-H shift from the $-CH_2$ group to the terminal oxygen leading to the

formation of S28-a (HO CHOOH) with the barrier of 41.6 kcal·mol^{-1}. $HOCH_2OO$-b can isomerize to S28-b1 and S28-b2 via the four-membered ring transition states TS34-b1 and TS34-b2 (1,3-H shifts) with the barriers of 41.6 and 45.0 kcal·mol^{-1}. But these three 1,3-H shift reactions have comparatively high barriers, making them irrelevant in the atmosphere. Despite many attempts, the transition states of H-shift reactions of $HOCH_2OO$-c and $HOCH_2OO$-d are not located. The result implies that the H-shift reactions of these two conformers are inhibited, which is consistent with the previous study that not all reactants will be in a conformation with a path across the barrier to reaction in the H-shift reactions of RO_2 radicals (Møller et al., 2016). Equivalent to the case of $HOCH_2OO$ radical, the isomerization of $HOCH(CH_3)OO$ radical proceeds via the 1,3- and 1,4-H shifts from the -CH or -CH_3 groups to the terminal oxygen resulting in formation of hydroperoxyalkyl radicals (Figure S13). These 1,3- and 1,4-H shift reactions accompany with the extremely high barriers (> 37.9 kcal·mol^{-1}), implying that they are of less importance in the atmosphere. Similar conclusion is also derived from the isomerization of $HO(CH_3)_2COO$ radical that 1,4-H shift reactions are unfavourable kinetically (Figure S14). The high barriers of 1,3- and 1,4-H shifts can be interpreted as the result of the large ring strain energy (RSE) in the cyclic transition state geometries. As a consequence, the isomerization reactions of $HOCH_2OO$, $HOCH(CH_3)OO$ and $HO(CH_3)_2COO$ radicals are not likely to proceed in the atmosphere.

The single-conformer rate coefficients ($k_{IRC\text{-}TST}$) and multi-conformer rate coefficients ($k_{MC\text{-}TST}$) of the isomerization of $HOCH_2OO$, $HOCH(CH_3)OO$ and $HOC(CH_3)_2OO$ radicals are calculated over the temperature range of 273-400 K as listed in Table S9-S11. As can be seen in Table S9, $k_{IRC\text{-}TST}$ of each conformer exhibits a marked positive temperature dependence over the temperature range studied. $k_{MC\text{-}TST}$ is significantly increased with rising temperature, implying that the temperature increasing is beneficial to the occurrence of $HOCH_2OO$ radical isomerization. Similar conclusion is also obtained from the isomerization of $HOCH(CH_3)OO$ and $HOC(CH_3)_2OO$ radicals (Table S10-S11). It is worth mentioning that $k_{MC\text{-}TST}$ is rapidly increased as the number of methyl group is increased. For

example, the room temperature $k_{MC\text{-}TST}$ of $HOCH_2OO$ radical isomerization is calculated to be 4.4 $\times 10^{-16}$ s^{-1}, which is lower than those of the $HOCH(CH_3)OO$ (2.9 $\times 10^{-13}$ s^{-1}) and $HO(CH_3)_2COO$ (3.0 $\times 10^{-12}$ s^{-1}) radicals isomerization by 660 and 6820 times, respectively.

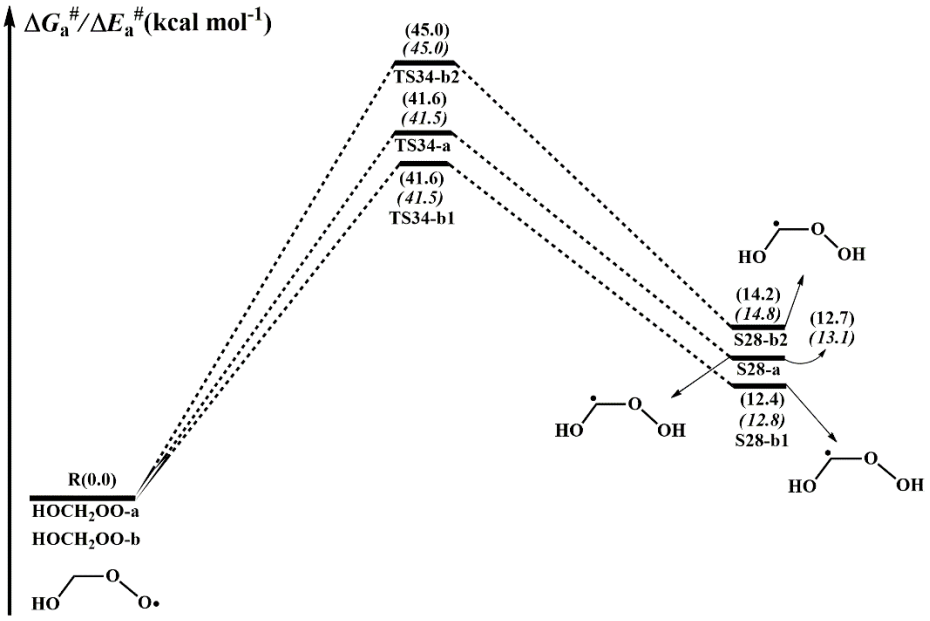

Figure 9. PES ($\Delta G_a^{\#}$ and $\Delta E_a^{\#}$, in italics) for the isomerization of $HOCH_2OO$ radical predicted at the M06-2X/ma-TZVP//M06-2X/6-311+G(2df,2p) level of theory

3.3 Subsequent reactions of H-abstraction products RO_2 radicals in urban environments

NO_x is present in high concentration in urban environments, reaction with NO is the dominant chemical sink for RO_2 radicals (Atkinson and Arey, 2003; Orlando and Tyndall, 2012; Perring et al., 2013). The main pathways in this type of reaction lead to the formation of NO_2, RO radicals, organic nitrites, and organic nitrate, and their formation yields are highly dependent on the nature of R group (Orlando and Tyndall, 2012). The formation of NO_2 through subsequent photolysis (λ < 420 nm) produces ozone and NO, increasing the concentrations of near-surface ozone and propagating NO_x chain (Orlando and Tyndall, 2012). The schematic PES for the reactions of distinct RO_2 radicals with NO are displayed in Figures 10-12. As shown in Figure 10, the bimolecular reaction between $HOCH_2OO$ radical and NO initially leads to nitrite adduct S31 via the barrierless addition of NO to terminal oxygen atom O_3 of $HOCH_2OO$ radical. The formed S31 exists two isomers: S31-*cis* refers to the O_2 and

O_4 on the same side ($DO_2O_3N_1O_4$ = 2.3 °), whereas S31-*trans* refers to the O_2 and O_4 on the opposite side ($DO_2O_3N_1O_4$ = -179.8 °) with respect to the O_3-N_1 bond. The calculations show that S31-*cis* is more stable than S31-*trans* by 1.1 kcal mol^{-1} in energy. The tautomerization between S31-*cis* and S31-*trans* proceeds through the rotating of O_3-N_1 bond with the barrier of 14.4 kcal mol^{-1}, implying that they can be regarded as the separate atmospheric species. According to the Boltzmann-weighted distribution, at room temperature, the predicted percentages of S31-*cis* and S31-*trans* are 86.5% and 13.5%, respectively. The result implies that the dominant product of $HOCH_2OO$ radical reaction with NO is S31-*cis*, and it is selected as a model compound to insight into the mechanism of secondary reactions in the following sections.

S31-*cis* can either isomerize to organic nitrate S32 (R38) via the O_2-O_3 bond breaking and O_2-N_1 bond forming with the barrier of 47.8 kcal mol^{-1}, or decompose into $HOCH_2O$ radical and NO_2 (R39) via the cleavage of O_2-O_3 bond with the barrier of 11.3 kcal mol^{-1}. The result shows that the latter pathway is more favourable than the former channel due to its lower barrier. It should be noted that the corresponding transition state TS39 is not located using M06-2X functional, but it is located at the MP2/6-311+G(2df,2p) level of theory and is verified using IRC calculations. The formed $HOCH_2O$ radical has two kinds of pathways: (1) it directly decomposes into CH_2O and OH radical (R40) via β-site C_1-O_1 bond scission with the barrier of 52.4 kcal mol^{-1}; (2) it converts into HCOOH and HO_2 radical (R41) through H-abstraction by O_2 with the barrier of 26.4 kcal mol^{-1}. This result reveals that R41 is the most feasible channel in the fragmentation of $HOCH_2O$ radical.

From Figure 11, it can be seen that the addition NO to $HOCH(CH_3)OO$ radical leading to the formation of S33-*cis* is barrierless. Then, it decomposes into $HOCH(CH_3)O$ radical and NO_2 (R44) via the cleavage of O_2-O_3 bond with the barrier of 11.5 kcal mol^{-1}. The resulting $HOCH(CH_3)O$ radical has three types of pathways. The first one is β-site C_1-C_2 bond scission leading to the formation of HCOOH + CH_3 (R45) with the barrier of 8.3 kcal mol^{-1}. The second one is β-site C_1-O_1 bond cleavage resulting in formation of CH_3COH + OH (R46) with the barrier of 26.7

637 kcal mol^{-1}. The third one is H-abstraction by O_2 leading to $CH_3COOH + HO_2\cdot$ (R47)
638 with the barrier of 26.2 kcal mol^{-1}. Based on the calculated reaction barriers, it can be
639 found that β-site C_1-C_2 bond scission is the dominant pathway in the fragmentation of
640 $HOCH(CH_3)O$ radical. This conclusion is further supported by the previous
641 experimental result that β-hydroxy intermediates primarily proceed decomposition
642 rather than react with O_2 in the presence of NO (Aschmann et al., 2000). Equivalent to
643 the $HOCH(CH_3)OO\cdot$ + NO reaction, the bimolecular reaction of $HO(CH_3)_2COO$
644 radical with NO has similar transformation pathways (Figure 12). The reaction for
645 $HO(CH_3)_2COO$ with NO initially proceeds via a barrierless addition leading to
646 S35-*cis* with the binding energy of 12.6 kcal mol^{-1}. Then, S35-*cis* fragments into
647 $HO(CH_3)_2CO$ radical along with NO_2 (R50) via the cleavage of O_2-O_3 bond with the
648 barrier of 11.4 kcal mol^{-1}. The formed $HO(CH_3)_2CO$ radical can either dissociate to
649 $CH_3COOH + CH_3\cdot$ (R51) via the C_1-C_3 bond scission with the barrier of 8.2
650 kcal mol^{-1}, or decompose into CH_3COCH_3 + OH (R52) through the C_1-O_1 bond
651 breaking with the barrier of 24.3 kcal mol^{-1}. The result again shows that the β-site
652 C-C bond scission is the dominate pathway.

653 The typical atmospheric concentrations of NO are about 10 ppbv, 1 ppbv and 20
654 pptv in the urban, rural and forest environments (Bianchi et al., 2019). The rate
655 coefficient of $HOCH_2OO\cdot$ reaction with NO is calculated to be 4.3×10^{-12} cm^3
656 molecule^{-1} s^{-1} at room temperature, resulting in the pseudo-first-order rate constants
657 $k'_{NO} = k_{NO}[NO]$ of 6.5×10^{-1}, 6.5×10^{-2}, and 1.3×10^{-3}, respectively, in the urban,
658 rural and forest environments. It is of interest to assess the relative importance for the
659 H-shift reaction of $HOCH_2OO$ radical and bimolecular reactions with $HO_2\cdot$ and NO
660 based on the calculated $k_{MC\text{-}TST}$, k'_{HO2} and k'_{NO}. It can be found that the H-shift
661 reaction is of less importance, the HO_2 radical reaction is favorable in the forest
662 environment, while the NO reaction is predominant in the urban and rural regions.
663 Similar conclusion is also obtained from the cases of $HOCH(CH_3)OO$ and
664 $HO(CH_3)_2CHOO$ radicals.

665 The rate coefficients of the dominant pathways of $HOCH_2O$, $HOCH(CH_3)O$ and
666 $HO(CH_3)_2CHO$ radicals fragmentation are summarized in Table S12. As can be seen

in Table S12, k_{R41} is slightly increased with the temperature increasing, and the discrepancy is about a factor of 12 at the two extremes of temperature. At ground level with $[O_2]$ = ~ 5.0 × 10^{18} molecule cm^{-3}, the pseudo-first-order rate constant k'_{O2} = $k_{R41}[O_2]$ is estimated to be 38.0 s^{-1} at room temperature. k_{R45} vary significantly from 2.0 × 10^6 (273 K) to 3.1 × 10^8 (400 K) s^{-1}, and they exhibit a marked positive temperature dependence. Similar phenomenon is also observed from k_{R51} that k_{R51} is significantly increased with increasing temperature. k_{R51} is a factor of ~ 1.3 greater than k_{R45} in the temperature range studied, implying that the rate coefficient of β-site C-C bond scission is slightly increased as the number of methyl group is increased.

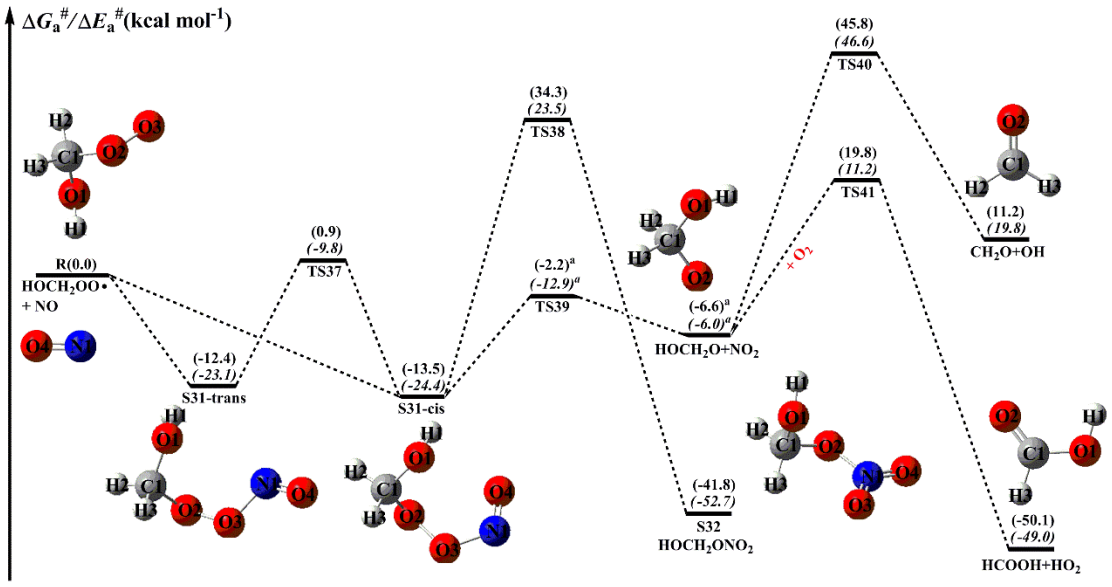

Figure 10. PES ($\Delta G_a^{\#}$ and $\Delta E_a^{\#}$, in italics) for the reaction of $HOCH_2OO$ radical with NO predicted at the M06-2X/ma-TZVP//M06-2X/6-311+G(2df,2p) level of theory (the superscript a is calculated at the MP2/ma-TZVP//MP2/6-311+G(2df,2p) level)

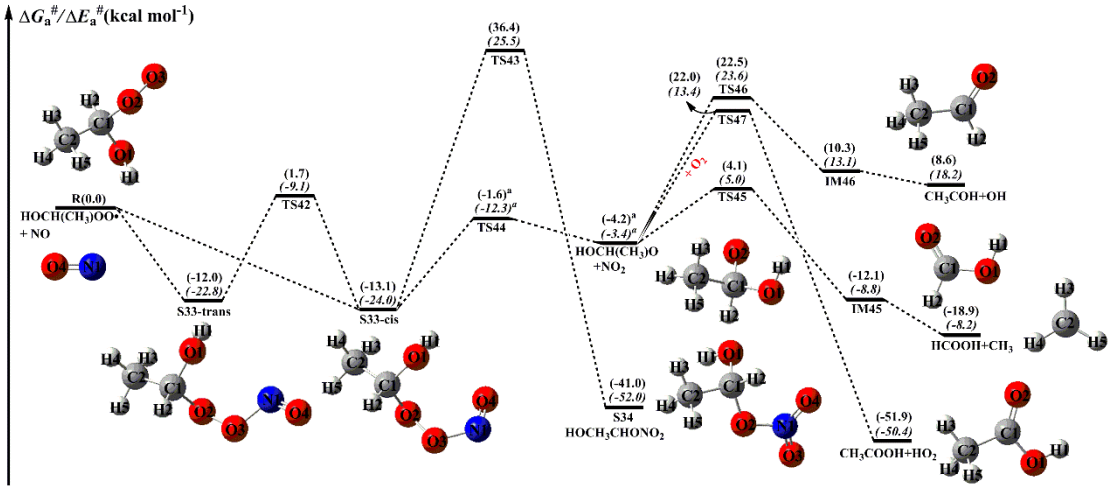

682

683 **Figure 11.** PES ($\Delta G_a^{\#}$ and $\Delta E_a^{\#}$, in italics) for the reaction of $HOCH(CH_3)OO$ radical with NO
684 predicted at the M06-2X/ma-TZVP//M06-2X/6-311+G(2df,2p) level of theory (the superscript a is
685 calculated at the MP2/ma-TZVP//MP2/6-311+G(2df,2p) level)

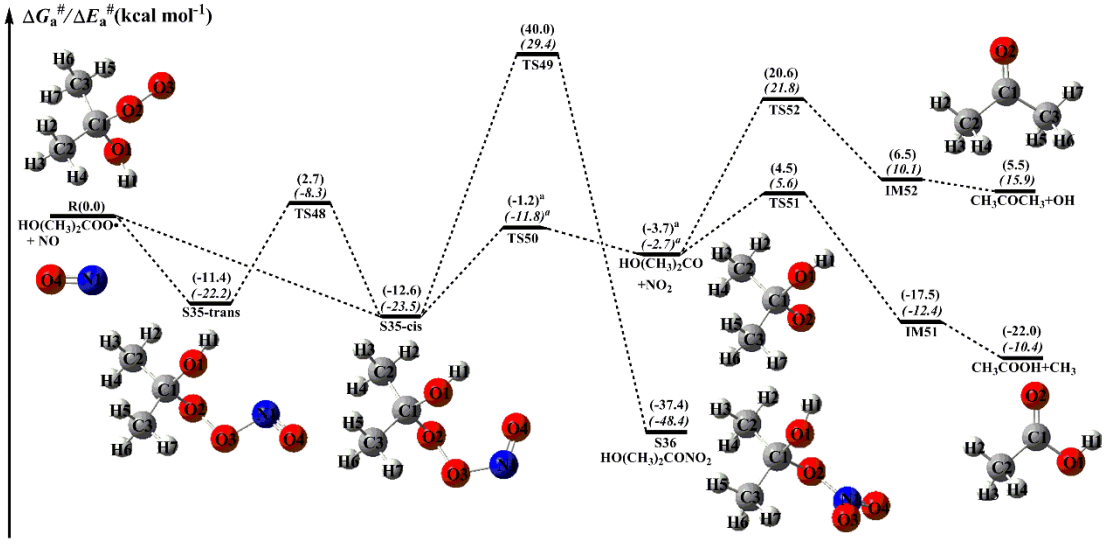

686

687 **Figure 12.** PES ($\Delta G_a^{\#}$ and $\Delta E_a^{\#}$, in italics) for the reaction of $HO(CH_3)_2COO$ radical with NO
688 predicted at the M06-2X/ma-TZVP//M06-2X/6-311+G(2df,2p) level of theory (the superscript a is
689 calculated at the MP2/ma-TZVP//MP2/6-311+G(2df,2p) level)

690 # 4. Conclusions

691 The detailed mechanisms and kinetic properties of OH-initiated oxidation of
692 distinct HHPs and subsequent transformation of resulting H-abstraction products are
693 investigated using quantum chemical and kinetics modeling methods. The main
694 conclusions are summarized as follows:

695 (a) The dominant pathway is the H-abstraction from the -OOH group in the
696 initiation reactions of OH radical with $HOCH_2OOH$ and $HOC(CH_3)_2OOH$.
697 H-abstraction from -CH group is competitive with that from the -OOH group in the

reaction of OH radical with $HOCH(CH_3)OOH$. The barrier of H-abstraction from the -OOH group is slightly increased as the number of methyl group is increased. Compared with the rate coefficient of dominant pathway in the parent system, it is almost identical when a methyl group substitution occurs at the C_1-position, whereas it reduces by a factor of 2-5 when two methyl groups introduce into the C_1-position.

(b) The self-reaction of H-abstraction product RO_2 radical initially produces tetroxide intermediate via an oxygen-to-oxygen coupling, then it decomposes into propagation and termination products through the asymmetric two-step O-O bond scission. The rate-limiting step is the first O-O bond cleavage, and the barrier is increased with increasing the number of methyl group.

(c) The bimolecular reactions of distinct RO_2 radicals with HO_2 radical lead to the formation of hydroperoxide ROOH as the main product, and the barrier height is independent on the number of methyl substitution. The calculated rate coefficients exhibit a weakly negative temperature dependence, translating into the pseudo-first-order rate constant k'_{HO2} of 1-5 $\times 10^{-2}$ s^{-1} in the forest environments.

(d) Reaction with O_2 forming formic acid and HO_2 radical is the dominant removal pathway for $HOCH_2O$ radical formed from the reaction of $HOCH_2OO$ radical with NO. The β-site C-C bond scission is the dominate pathway in the dissociation of $HOCH(CH_3)O$ and $HOC(CH_3)_2O$ radicals formed from the $HOCH(CH_3)OO\cdot$ + NO and $HOC(CH_3)_2OO\cdot$ + NO reactions.

Data availability

The data are accessible by contacting the corresponding author (huangyu@ieecas.cn).

Supplement

The following information is provided in the Supplement: Y//X (Y = M06-2X, CCSD(T), X = 6-311+G(2df,2p), ma-TZVP) calculated energy barrier ($\Delta E_a^{\#}$, $\Delta G_a^{\#}$) for OH + HHPs reactions; Rate coefficients of every elementary pathway involved in

the initial reactions of OH radical with $HOCH_2OOH$, $HOCH(CH_3)OOH$ and $HO(CH_3)_2COOH$; Rate coefficients of HO_2 radical reactions with $HOCH_2OO$, $HOCH(CH_3)OO$ and $HO(CH_3)_2COO$ radicals; The relative free energy and Boltzmann populations (w_i) of the conformer of $HOCH_2OO$, $HOCH(CH_3)OO$ and $HO(CH_3)_2COO$ radicals; The single-conformer rate coefficients ($k_{IRC\text{-}TST}$) and multi-conformer rate coefficients ($k_{MC\text{-}TST}$) of $HOCH_2OO$, $HOCH(CH_3)OO$ and $HO(CH_3)_2COO$ radicals; Rate coefficients of dominant pathways in the $HOCH_2OO\cdot$ + NO, $HOCH(CH_3)OO\cdot$ + NO and $HO(CH_3)_2CHOO\cdot$ + NO reactions; PESs ($\Delta E_a^{\#}$) for the OH-initiated reactions of $HOCH_2OOH$, $HOCH(CH_3)OOH$, $HOC(CH_3)_2OOH$; Geometries of all the stationary points; Plots of the rate coefficients of every elementary pathway versus temperature; PESs ($\Delta G_a^{\#}$ and $\Delta E_a^{\#}$, in italics) for the isomerization of $HOCH(CH_3)OO$ and $HO(CH_3)_2COO$ radicals.

Author contribution

LC designed the study. LC and YH wrote the paper. LC performed theoretical calculation. YX, ZJ, and WW analyzed the data. All authors reviewed and commented on the paper.

Competing interests

The authors declare that they have no conflict of interest.

Acknowledgments

This work was supported by the National Natural Science Foundation of China (grant Nos. 42175134, 41805107, and 22002080). It was also partially supported as Key Projects of Chinese Academy of Sciences, China (grant No. ZDRW-ZS-2017-6), Strategic Priority Research Program of the Chinese Academy of Sciences, China (grant Nos. XDA23010300 and XDA23010000), Key Project of International Cooperation of the Chinese Academy of Sciences, China (grant No. GJHZ1543),

Research Grants Council of Hong Kong, China (grant No. PolyU 152083/14E), CAS "Light of West China" Program (XAB2019B01) and the General Project of Shaanxi Province (2020JQ-432).

References

Allen, H. M., Crounse, J. D., Bates, K. H., Teng, A. P., Krawiec-Thayer, M. P., Rivera-Rios, J. C., Keutsch, F. N., Clair, J. M. S., Hanisco, T. F., Møller, K. H., Kjaergaard, H. G., and Wennberg, P. O.: Kinetics and product yields of the OH initiated oxidation of hydroxymethyl hydroperoxide, J. Phys. Chem. A, 122, 6292-6302, https://doi.org/10.1021/acs.jpca.8b04577, 2018.

Anglada, J. M., and Solé, A.: Impact of the water dimer on the atmospheric reactivity of carbonyl oxides, Phys. Chem. Chem. Phys., 18, 17698-17712, https://doi.org/10.1039/C6CP02531E, 2016.

Anglada, J. M., González, J., and Torrent-Sucarrat, M.: Effects of the substituents on the reactivity of carbonyl oxides. a theoretical study on the reaction of substituted carbonyl oxides with water, Phys. Chem. Chem. Phys., 13, 13034-13045, https://doi.org/10.1039/c1cp20872a, 2011.

Aschmann, S. M., Arey, J., and Atkinson, R.: Formation of β-hydroxycarbonyls from the OH radical-initiated reactions of selected alkenes, Environ. Sci. Technol., 34, 1702-1706, https://doi.org/10.1021/es991125a, 2000.

Atkinson, R., and Arey, J.: Atmospheric degradation of volatile organic compounds, Chem. Rev., 103, 4605-4638, https://doi.org/10.1021/cr0206420, 2003.

Bach, R. D., Dmitrenko, O., and Estévez, C. M.: Chemical behavior of the biradicaloid (HO ··ONO) singlet states of peroxynitrous acid. the oxidation of hydrocarbons, sulfides, and selenides, J. Am. Chem. Soc., 127, 3140-3155, https://doi.org/10.1021/ja044245d, 2005.

Berndt, T., Richters, S., Kaethner, R., Voigtländer, J., Stratmann, F., Sipilä, M., Kulmala, M., and Herrmann, H.: Gas-phase ozonolysis of cycloalkenes: formation of highly oxidized RO_2 radicals and their reactions with NO, NO_2, SO_2, and Other RO_2 radicals, J. Phys. Chem. A, 119, 10336-10348, https://doi.org/10.1021/acs.jpca.5b07295, 2015.

Berndt, T., Scholz, W., Mentler, B., Fischer, L., Herrmann, H., Kulmala, M., and Hansel, A.: Accretion product formation from self- and cross-reactions of RO_2 radicals in the atmosphere, Angew. Chem. Int. Ed., 57, 3820-3824, https://doi.org/10.1002/anie.201710989, 2018.

Bianchi, F., Kurten, T., Riva, M., Mohr, C., Rissanen, M. P., Roldin, P., Berndt, T., Crounse, J. D., Wennberg, P. O., Mentel, T. F., Wildt, J., Junninen, H., Jokinen, T., Kulmala, M., Worsnop, D. R., Thornton, J. A., Donahue, N., Kjaergaard, H. G., and Ehn, M.: Highly oxygenated organic molecules (HOM) from gas-phase autoxidation involving peroxy radicals: a key contributor to atmospheric aerosol, Chem. Rev., 119, 3472-3509, https://doi.org/10.1021/acs.chemrev.8b00395, 2019.

Boys, S. F., and Bernardi, F.: The calculation of small molecular interactions by the differences of separate total energies. Some procedures with reduced errors, Mol. Phys., 19, 553-566, https://doi.org/10.1080/00268977000101561, 1970.

Chao, W., Hsieh, J. T., Chang, C. H., and Lin, J. J. M.: Direct kinetic measurement of the reaction of the simplest Criegee intermediate with water vapor, Science, 347, 751-754, https://doi.org/10.1126/science.1261549, 2015.

Chen, L., Huang, Y., Xue, Y., Cao, J., and Wang, W.: Competition between HO_2 and H_2O_2 reactions with CH_2OO/*anti*-CH_3CHOO in the oligomer formation: a theoretical perspective, J. Phys. Chem. A, 121, 6981-6991, https://doi.org/10.1021/acs.jpca.7b05951, 2017.

Chen, L., Huang, Y., Xue, Y., Jia, Z., and Wang, W.: Atmospheric oxidation of 1-butene initiated by OH radical: Implications for ozone and nitrous acid formations, Atmos. Environ., 244, 118010-118021, https://doi.org/10.1016/j.atmosenv.2020.118010, 2021.

Chen, L., Huang, Y., Xue, Y., Shen, Z., Cao, J., and Wang, W.: Mechanistic and kinetics investigations of oligomer formation from Criegee intermediate reactions with hydroxyalkyl hydroperoxides, Atmos. Chem. Phys., 19, 4075-4091, https://doi.org/10.5194/acp-19-4075-2019, 2019.

Chen, L., Wang, W., Wang, W., Liu, Y., Liu, F., Liu, N., and Wang, B.: Water-catalyzed decomposition of the simplest Criegee intermediate CH_2OO, Theor. Chem. Acc., 135, 131-143, https://doi.org/10.1007/s00214-016-1894-9, 2016b.

Chen, L., Wang, W., Zhou, L., Wang, W., Liu, F., Li, C., and Lü, J.: Role of water clusters in the reaction of the simplest Criegee intermediate CH_2OO with water vapour, Theor. Chem. Acc., 135, 252-263, https://doi.org/10.1007/s00214-016-1998-2, 2016a.

Chhantyal-Pun, R., Welz, O., Savee, J. D., Eskola, A. J., Lee, E. P. F., Blacker, L., Hill, H. R., Ashcroft, M., Khan, M. A. H., Lloyd-Jones, G. C., Evans, L., Rotavera, B., Huang, H., Osborn, D. L., Mok, D. K. W., Dyke, J. M., Shallcross, D. E., Percival, C. J., Orr-Ewing, A. J., and Taatjes, C. A.: Direct measurements of unimolecular and bimolecular reaction kinetics of the Criegee intermediate $(CH_3)_2COO$, J. Phys. Chem. A, 121, 4-15, https://doi.org/10.1021/acs.jpca.6b07810, 2017.

Crounse, J. D., Nielsen, L. B., Jørgensen, S., Kjaergaard, H. G., and Wennberg, P. O.: Autoxidation of organic compounds in the atmosphere, J. Phys. Chem. Lett., 4, 3513-3520, https://doi.org/10.1021/jz4019207, 2013.

Dillon, T. J., and Crowley, J. N.: Direct detection of OH formation in the reactions of HO_2 with $CH_3C(O)O_2$ and other substituted peroxy radicals, Atmos. Chem. Phys., 8, 4877-4889, https://doi.org/10.5194/acp-8-4877-2008, 2008.

Eckart, C.: The penetration of a potential barrier by electrons, Phys. Rev., 35, 1303-1309, https://doi.org/10.1103/PhysRev.35.1303, 1930.

Ehn, M., Berndt, T., Wildt, J., and Mentel, T.: Highly oxygenated molecules from atmospheric autoxidation of hydrocarbons: a prominent challenge for chemical kinetics studies, Int. J. Chem. Kinet., 49, 821-831, https://doi.org/10.1002/kin.21130, 2017.

Ehn, M., Thornton, J. A., Kleist, E., Sipilä, M., Junninen, H., Pullinen, I., Springer, M., Rubach, F., Tillmann, R., Lee, B., Lopez-Hilfiker, F., Andres, S., Acir, I. H., Rissanen, M., Jokinen,T., Schobesberger, S., Kangasluoma, J., Kontkanen, J., Nieminen, T., Kurtén, T., Nielsen, L. B., Jørgensen, S., Kjaergaard, H. G., Canagaratna, M., Maso, M. D., Berndt, T., Petäjä, T., Wahner, A., Kerminen, V. M., Kulmala, M., Worsnop, D. R., Wildt, J., and Mentel T. F.: A large source of low-volatility secondary organic aerosol, Nature, 506, 476-479, https://doi.org/10.1038/nature13032, 2014.

Fernández-Ramos, A., Ellingson, B. A., Meana-Pañeda, R., Marques, J. M. C., and Truhlar, D. G.:

Symmetry numbers and chemical reaction rates, Theor. Chem. Acc., 118, 813-826, https://doi.org/10.1007/s00214-007-0328-0, 2007.

Francisco, J. S., and Eisfeld, W.: Atmospheric oxidation mechanism of hydroxymethyl hydroperoxide, J. Phys. Chem. A, 113, 7593-7600, https://doi.org/10.1021/jp901735z, 2009.

Frisch, M. J., Trucks, G. W., Schlegel, H. B., Scuseria, G. E., Robb, M. A., Cheeseman, J. R., Montgomery, J. A. Jr., Vreven, T., Kudin, K. N., Burant, J. C., Millam, J. M., Iyengar, S. S., Tomasi, J., Barone, V., Mennucci. B., Cossi, M., Scalmani, G., Rega, N., Petersson, G. A., Nakatsuji, H., Hada, M., Ehara, M., Toyota, K., Fukuda, R., Hasegawa, J., Ishida, M., Nakajima, T., Honda, Y., Kitao, O., Nakai, H., Klene, M., Li, X., Knox, J. E., Hratchian, H. P., Cross, J. B., Adamo, C., Jaramillo, J., Gomperts, R., Stratmann, R. E., Yazyev, O., Austin, A. J., Cammi, R., Pomelli, C., Ochterski, J. W., Ayala, P. Y., Morokuma, K., Voth, G. A., Salvador, P., Dannenberg, J. J., Zakrzewski, V. G., Dapprich, S., Daniels, A. D., Strain, M. C., Farkas, O., Malick, D. K., Rabuck, A. D., Raghavachari, K., Foresman, J. B., Ortiz, J. V., Cui, Q., Baboul, A. G., Clifford, S., Cioslowski, J., Stefanov, B. B., Liu, G., Liashenko, A., Piskorz, P., Komaromi, I., Martin, R. L., Fox, D. J., Keith, T., Al-Laham, M. A., Peng, C. Y., Nanayakkara, A., Challacombe, M., Gill, P. M. W., Johnson, B., Chen, W., Wong, M. W., Gonzalez, C., and Pople, J. A.: Gaussian 09, Revision D.01; Gaussian, Inc.: Wallingford, CT, 2009.

Fukui, K.: The path of chemical reactions - the IRC approach, Acc. Chem. Res., 14, 363-368, https://doi.org/10.1021/ar00072a001, 1981.

Gilbert, R. G., and Smith, S. C.: Theory of unimolecular and recombination reactions; Blackwell Scientific: Carlton, Australia, 1990.

Gligorovski, S., Strekowski, R., Barbati, S., and Vione, D.: Environmental implications of hydroxyl radicals (OH), Chem. Rev., 115, 13051-13092, https://doi.org/10.1021/cr500310b, 2015.

Glowacki, D. R., Liang, C. H., Morley, C., Pilling, M. J., and Robertson, S. H.: MESMER: an open-source master equation solver for multi-energy well reactions, J. Phys. Chem. A, 116, 9545-9560, https://doi.org/10.1021/jp3051033, 2012.

Gong, Y., and Chen, Z.: Quantification of the role of stabilized Criegee intermediates in the formation of aerosols in limonene ozonolysis, Atmos. Chem. Phys., 21, 813-829, https://doi.org/10.5194/acp-21-813-2021, 2021.

Hofzumahaus, A., Rohrer, F., Lu, K., Bohn, B., Brauers, T., Chang, C. C., Fuchs, H., Holland, F., Kita, K., Kondo, Y., Li, X., Lou, S., Shao, M., Zeng, L., Wahner, A., and Zhang, Y.: Amplified trace gas removal in the troposphere, Science, 324, 1702-1704, https://doi.org/10.1126/science.1164566, 2009.

Holbrook, K. A., Pilling, M. J., Robertson, S. H., and Robinson, P. J.: Unimolecular reactions, 2nd ed.; Wiley: New York, 1996.

Huang, H. L., Chao, W., and Lin, J. J. M.: Kinetics of a Criegee intermediate that would survive high humidity and may oxidize atmospheric SO_2, Proc. Natl. Acad. Sci. U.S.A., 112, 10857-10862, https://doi.org/10.1073/pnas.1513149112, 2015.

Iyer, S., Reiman, H., Møller, K. H., Rissanen, M. P., Kjaergaard, H. G., and Kurtén, T.: Computational investigation of RO_2 + HO_2 and RO_2 + RO_2 reactions of monoterpene derived first-generation peroxy radicals leading to radical recycling, J. Phys. Chem. A, 122, 9542-9552, https://doi.org/10.1021/acs.jpca.8b09241, 2018.

Iyer, S., Rissanen, M. P., Valiev, R., Barua, S., Krechmer, J. E., Thornton, J., Ehn, M., and Kurtén, T.: Molecular mechanism for rapid autoxidation in α-pinene ozonolysis, Nat. Commun., https://doi.org/10.1038/s41467-021-21172-w, 12, 878-883, 2021.

Jara-Toro, R. A., Hernández, F. J., Garavagno, M. A., Taccone, R. A., and Pino, G. A.: Water catalysis of the reaction between hydroxyl radicals and linear saturated alcohols (ethanol and n-propanol) at 294 K, Phys. Chem. Chem. Phys., 20, 27885-27896, https://doi.org/10.1039/C8CP05411H, 2018.

Jara-Toro, R. A., Hernández, F. J., Taccone, R. A., Lane, S. I., and Pino, G. A.: Water catalysis of the reaction between methanol and OH at 294 K and the atmospheric implications, Angew. Chem., Int. Ed., 56, 2166-2170, https://doi.org/10.1002/anie.201612151, 2017.

Jokinen, T., Sipilä, M., Richters, S., Kerminen, V. M., Paasonen, P., Stratmann, F., Worsnop, D., Kulmala, M., Ehn, M., Herrmann, H., and Berndt, T.: Rapid autoxidation forms highly oxidized RO_2 radicals in the atmosphere, Angew. Chem. Int. Ed., 53, 14596-14600, https://doi.org/10.1002/anie.201408566, 2014.

Khan, M. A. H., Percival, C. J., Caravan, R. L., Taatjes, C. A., and Shallcross, D. E.: Criegee intermediates and their impacts on the troposphere, Environ. Sci.: Processes Impacts, 20, 437-453, https://doi.org/10.1039/C7EM00585G, 2018.

Kumar, M., and Francisco, J. S.: Red-light initiated decomposition of α-hydroxy methylperoxy radical in the presence of organic and inorganic acids: implications for the HO_x formation in the lower stratosphere, J. Phys. Chem. A, 120, 2677-2683, https://doi.org/10.1021/acs.jpca.6b01515, 2016.

Kumar, M., and Francisco, J. S.: Red-light-induced decomposition of an organic peroxy radical: a new source of the HO_2 radical, Angew. Chem. Int. Ed., 54, 15711-15714, https://doi.org/10.1002/anie.201509311, 2015.

Kumar, M., Busch, D. H., Subramaniam, Bala., and Thompson, W. H.: Role of tunable acid catalysis in decomposition of α-hydroxyalkyl hydroperoxides and mechanistic implications for tropospheric chemistry, J. Phys. Chem. A, 118, 9701-9711, https://doi.org/10.1021/jp505100x, 2014.

Lee, R., Gryn'ova, G., Ingold, K. U., and Coote, M. L.: Why are sec-alkylperoxyl bimolecular self-reactions orders of magnitude faster than the analogous reactions of tert-alkylperoxyls? The unanticipated role of CH hydrogen bond donation, Phys. Chem. Chem. Phys., 18, 23673-23679, https://doi.org/10.1039/C6CP04670C, 2016.

Lester, M. I., and Klippenstein, S. J.: Unimolecular decay of Criegee intermediates to OH radical products: prompt and thermal decay processes, Acc. Chem. Res., 51, 978-985, https://doi.org/10.1021/acs.accounts.8b00077, 2018.

Liu, L., Bei, N., Wu, J., Liu, S., Zhou, J., Li, X., Yang, Q., Feng, T., Cao, J., Tie, X., and Li, G.: Effects of stabilized Criegee intermediates (sCIs) on sulfate formation: a sensitivity analysis during summertime in Beijing-Tianjin-Hebei (BTH), China. Atmos. Chem. Phys., 19, 13341-13354, https://doi.org/10.5194/acp-19-13341-2019, 2019.

Long, B., Bao, J. L., and Truhlar, D. G.: Reaction of SO_2 with OH in the atmosphere, Phys. Chem. Chem. Phys., 19, 8091-8100, https://doi.org/10.1039/C7CP00497D, 2017.

Lu, T.: Molclus program, Version 1.9.3, http://www.keinsci.com/research/molclus.html (accessed Feb. 10, 2020).

Ma, F., Guo, X., Xia, D., Xie, H. B., Wang, Y., Elm, J., Chen, J., and Niu, J.: Atmospheric

chemistry of allylic radicals from isoprene: a successive cyclization-driven autoxidation mechanism, Environ. Sci. Technol., 55, 4399-4409, https://doi.org/10.1021/acs.est.0c07925, 2021.

Møller, K. H., Berndt, T., and Kjaergaard, H. G.: Atmospheric autoxidation of amines, Environ. Sci. Technol., 54, 11087-11099, https://doi.org/10.1021/acs.est.0c03937, 2020.

Møller, K. H., Otkjær, R. V., Hyttinen, N., Kurtén, T., and Kjaergaard, H. G.: Cost-effective implementation of multiconformer transition state theory for peroxy radical hydrogen shift reactions, J. Phys. Chem. A, 120, 10072-10087, https://doi.org/10.1021/acs.jpca.6b09370, 2016.

Nozière, B., and Vereecken, L.: Direct observation of aliphatic peroxy radical autoxidation and water effects: an experimental and theoretical study, Angew. Chem. Int. Ed., 58, 13976-13982, https://doi.org/10.1002/anie.201907981, 2019.

Orlando, J. J., and Tyndall, G. S.: Laboratory studies of organic peroxy radical chemistry: an overview with emphasis on recent issues of atmospheric significance, Chem. Soc. Rev., 41, 6294-6317, https://doi.org/10.1039/c2cs35166h, 2012.

Perring, A. E., Pusede, S. E., and Cohen, R. C.: An observational perspective on the atmospheric impacts of alkyl and multifunctional nitrates on ozone and secondary organic aerosol, Chem. Rev., 113, 5848-5870, https://doi.org/10.1021/cr300520x, 2013.

Qiu, J. T., Ishizuka, S., Tonokura, K., Colussi, A. J., and Enami, S.: Water dramatically accelerates the decomposition of α-hydroxyalkyl-hydroperoxides in aerosol particles, J. Phys. Chem. Lett., 10, 5748-5755, https://doi.org/10.1021/acs.jpclett.9b01953, 2019.

Rissanen, M. P., Kurtén, T., Sipilä, M., Thornton, J. A., Kangasluoma, J., Sarnela, N., Junninen, H., Jørgensen, S., Schallhart, S., Kajos, M. K., Taipale, R., Springer, M., Mentel, T. F., Ruuskanen, T., Petäjä, T., Worsnop, D. R., Kjaergaard, H. G., and Ehn, M.: The formation of highly oxidized multifunctional products in the ozonolysis of cyclohexene, J. Am. Chem. Soc., 136, 15596-15606, https://doi.org/10.1021/ja507146s, 2014.

Russell, G. A.: Deuterium-isotope effects in the autoxidation of aralkyl hydrocarbons. Mechanism of the interaction of peroxy radicals, J. Am. Chem. Soc., 79, 3871-3877, https://doi.org/10.1021/ja01571a068, 1957.

Ryzhkov, A. B., and Ariya, P. A.: A theoretical study of the reactions of carbonyl oxide with water in atmosphere: the role of water dimer, Chem. Phys. Lett., 367, 423-429, https://doi.org/10.1016/S0009-2614(02)01685-8, 2003.

Smith, M. C., Chang, C. H., Chao, W., Lin, L. C., Takahashi, K., Boering, K. A., and Lin, J. J. M.: Strong negative temperature dependence of the simplest Criegee intermediate CH_2OO reaction with water dimer, J. Phys. Chem. Lett., 6, 2708-2713, https://doi.org/10.1021/acs.jpclett.5b01109, 2015.

Stone, D., Whalley, L. K., and Heard, D. E.: Tropospheric OH and HO_2 radicals: field measurements and model comparisons, Chem. Soc. Rev., 41, 6348-6404, https://doi.org/10.1039/c2cs35140d, 2012.

Taatjes, C. A., Welz, O., Eskola, A. J., Savee, J. D., Scheer, A. M., Shallcross, D. E., Rotavera, B., Lee, E. P. F., Dyke, J. M., Mok, D. K. W., Osborn, D. L., and Percival, C. J.: Direct measurements of conformer-dependent reactivity of the Criegee intermediate CH_3CHOO, Science, 340, 177-180, https://doi.org/10.1126/science.1234689, 2013.

Taatjes, C. A.: Criegee intermediates: what direct production and detection can teach us about

reactions of carbonyl oxides, Annu. Rev. Phys. Chem., 68, 183-207, https://doi.org/10.1146/annurev-physchem-052516-050739, 2017.

Valiev, R. R., Hasan, G., Salo, V. T., Kubečka, J., and Kurten, T.: Intersystem crossings drive atmospheric gas-phase dimer formation, J. Phys. Chem. A, 123, 6596-6604, https://doi.org/10.1021/acs.jpca.9b02559, 2019.

Wang, S., Riva, M., Yan, C., Ehn, M., and Wang, L.: Primary formation of highly oxidized multifunctional products in the OH-initiated oxidation of isoprene: a combined theoretical and experimental study, Environ. Sci. Technol., 52, 12255-12264, https://doi.org/10.1021/acs.est.8b02783, 2018.

Wang, S., Wu, R., Berndt, T., Ehn, M., and Wang, L.: Formation of highly oxidized radicals and multifunctional products from the atmospheric oxidation of alkylbenzenes, Environ. Sci. Technol., 51, 8442-8449, https://doi.org/10.1021/acs.est.7b02374, 2017.

Wennberg, P. O., Bates, K. H., Crounse, J. D., Dodson, L. G., McVay, R. C., Mertens, L. A., Nguyen, T. B., Praske, E., Schwantes, R. H., Smarte, M. D., Clair, J. M. S., Teng, A. P., Zhang, X., and Seinfeld, J. H.: Gas-phase reactions of isoprene and its major oxidation products, Chem. Rev., 118, 3337-3390, https://doi.org/10.1021/acs.chemrev.7b00439, 2018.

Winiberg, F. A. F., Dillon, T. J., Orr, S. C., Groß, C. B. M., Bejan, I., Brumby, C. A., Evans, M. J., Smith, S. C., Heard, D. E., and Seakins, P. W.: Direct measurements of OH and other product yields from the $HO_2 + CH_3C(O)O_2$ reaction, Atmos. Chem. Phys., 16, 4023-4042, https://doi.org/10.5194/acp-16-4023-2016, 2016.

Xu, L., Kollman, M. S., Song, C., Shilling, J. E., and Ng, N. L.: Effects of NO_x on the volatility of secondary organic aerosol from isoprene photooxidation, Environ. Sci. Technol., 48, 2253-2262, https://doi.org/10.1021/es404842g, 2014.

Xu, L., Møller, K. H., Crounse, J. D., Kjaergaard, H. G., and Wennberg, P. O.: New insights into the radical chemistry and product distribution in the OH-initiated oxidation of benzene, Environ. Sci. Technol., 54, 13467-13477, https://doi.org/10.1021/acs.est.0c04780, 2020.

Zhang, P., Wang, W., Zhang, T., Chen, L., Du, Y., Li, C., and Lv, J.: Theoretical study on the mechanism and kinetics for the self-reaction of $C_2H_5O_2$ radicals, J. Phys. Chem. A, 116, 4610-4620, https://doi.org/10.1021/jp301308u, 2012.

Zhao, Y., and Truhlar, D. G.: A new local density functional for main-group thermochemistry, transition metal bonding, thermochemical kinetics, and noncovalent interactions, J. Chem. Phys., 125, 194101-194119, https://doi.org/10.1063/1.2370993, 2006.

Zhao, Y., and Truhlar, D. G.: The M06 suite of density functionals for main group thermochemistry, thermochemical kinetics, noncovalent interactions, excited states, and transition elements: two new functionals and systematic testing of four M06-class functionals and 12 other functionals, Theor. Chem. Acc., 120, 215-241, https://doi.org/10.1007/s00214-007-0310-x, 2008.

Zheng, J., and Truhlar, D. G.: Direct dynamics study of hydrogen-transfer isomerization of 1-pentyl and 1-hexyl radicals, J. Phys. Chem. A, 113, 11919-11925, https://doi.org/10.1021/jp903345x, 2009.

Zheng, J., Xu, X., and Truhlar, D. G.: Minimally augmented Karlsruhe basis sets, Theor. Chem. Acc., 128, 295-305, https://doi.org/10.1007/s00214-010-0846-z, 2011.

Zhong, J., Kumar, M., Francisco, J. S., and Zeng, X. C.: Insight into chemistry on cloud/aerosol water surfaces, Acc. Chem. Res., 51, 1229-1237,

https://doi.org/10.1021/acs.accounts.8b00051, 2018.

Zhou, X., Liu, Y., Dong, W., and Yang, X.: Unimolecular reaction rate measurement of *syn*-CH_3CHOO, J. Phys. Chem. Lett., 10, 4817-4821, https://doi.org/10.1021/acs.jpclett.9b01740, 2019.

Zhu, C., Kumar, M., Zhong, J., Li, L., Francisco, J. S., and Zeng, X. C.: New mechanistic pathways for Criegee-water chemistry at the air/water interface, J. Am. Chem. Soc., 138, 11164-11169, https://doi.org/10.1021/jacs.6b04338, 2016.